REAL INSTITUTO Y OBSERVATORIO DE LA ARMADA EN SAN FERNANDO
BOLETÍN ROA N.º 2/2013

APLICACIÓN DEL SISTEMA GPS A LA SISMOLOGÍA: EL TERREMOTO DE LORCA

Leonor Mendoza Malia

MINISTERIO DE DEFENSA

REAL INSTITUTO Y OBSERVATORIO DE LA ARMADA EN SAN FERNANDO
BOLETÍN ROA No.2/2013

APLICACIÓN DEL SISTEMA GPS A LA SISMOLOGÍA: EL TERREMOTO DE LORCA

Fundación Alvargonzález

Real Instituto y Observatorio de la Armada

MINISTERIO
DE DEFENSA

CATÁLOGO GENERAL DE PUBLICACIONES OFICIALES
http://publicacionesoficiales.boe.es/

Edita:

MINISTERIO DE DEFENSA
SECRETARÍA GENERAL TÉCNICA

www.bibliotecavirtualdefensa.es

NIPO: 083-13-127-6 (impresión bajo demanda)
NIPO: 083-13-128-1 (edición en línea)
ISSN: 1131-5040
Fecha de edición: junio 2013

Foto portada:

Fachada del Edificio Principal del Real Instituto y Observatorio de la Armada (Siglo XVIII).

Esta memoria ha sido realizada como objeto de la beca concedida a la autora por la Fundación Alvargonzález en el año 2012.

La investigación llevada a cabo para desarrollar este trabajo se encuadra en los objetivos de los proyectos:
- Geociencias en Iberia: Estudios integrados de topografía y evolución 4D ("Topo-Iberia"), ref. CSD2006-00041.
- Sistema de alerta sísmica temprana: Aplicación al Sur de España ("ALERT-ES"), ref. CGL2010-19803-C03-02.

Debido a la importancia de los resultados presentados, y al ser considerado como un tema de interés actual, el proyecto aquí expuesto se ha desarrollado en inglés para facilitar su difusión internacional.

Contents

List of Tables

List of Figures

Abbreviations

ART: Aspect Repeat Time
ASPREP: Program to calculate the ART
BPE: Bernese Processing Engine
CDDIS: Crustal Dynamics Data Information System
CGPS: Continuous GPS
CODE: Center for Orbit Determination in Europe
CRTG: GPS Station at Cartagena
CRVC: GPS Station at Caravaca de la Cruz
DD: Double Differencing
DOY: Day of Year
ERP: Earth Rotation Parameters
EUREF: European Reference Frame
FTP: File Transfer Protocol
GLONASS: Global Navigation Satellite Systems
GPS: Global Positioning System
GPST: GPS Time
IGN: Instituto Geográfico Nacional (National Geographical Institute, Spain)
IGS: International GNSS Service
IGS-RTPP: IGS Real-Time Pilot Project
JUMI: GPS Station at Jumilla
LORC: GPS Station at Lorca
Meristemum: Consejería de Agricultura y Agua of the Murcia Region GPS Network
MJD: Modified Julian Date
MSF: Modified Sidereal Filter
MURC: GPS Station at Murcia
NTRIP: Networked Transport of RTCM Data via Internet Protocol
PPP: Precise Point Positioning
RINEX: Receiver-INdependent Exchange
RF: Regional Filter
ROA: Real Instituto y Observatorio de la Armada en San Fernando (San Fernando Naval Observatory)
RTCM: Radio Technical Commission for Maritime Services
SALI: GPS Station at San Pedro del Pinatar
SP3(-c): Extended Standard Product 3 Orbit Format
UCM: Universidad Complutense de Madrid (Madrid Complutense University)
UTC: Coordinated Universal Time

Beca Fundación Alvargonzález, año 2012

Motivación

La Península Ibérica, excluyendo los Pirineos y la cordillera Bética, está clasificada como una región continental estable. Sin embargo, se localiza cerca de la convergencia entre las placas Euroasiática y Africana (placa de Nubia), siendo la zona Azores-Gibraltar una región muy compleja y con potencial suficiente como para generar fuertes terremotos. Dentro de la Península, los mayores eventos de los que se tiene constancia histórica están comprendidos entre magnitudes M_W 6.9 y 7.1. Incluso se han encontrado evidencias de terremotos con magnitudes hasta M_W 7.3 en registros paleosísimicos [Vilanova et al., 2012]. El pasado terremoto de Lorca [Cabañas-Rodríguez et al., 2011] además de los últimos acontecimientos en Torreperogil (Jaén) [IGN, 2013] son dos ejemplos muy actuales de los daños que pueden llegar a producir eventos moderados.

Por otra parte, España es uno de los países en mayor riesgo en caso de la llegada de un maremoto, debido a la gran exposición costera así como a la alta densidad de población y por la importancia del turismo en tales zonas. En el pasado se han dado varios casos notables, como el terremoto Boumerdes-Zemmouri de 2003 (M_W 6.8) y el tsunami generado, que llegó a la costa Balear y provocó daños en la infraestructura de la zona. Un ejemplo histórico de gran impacto, y que podría repetirse, fue el maremoto generado a partir del conocido "Terremoto de Lisboa" de 1755, con epicentro en el Océano Atlántico a 200 km del Cabo San Vicente. Esta ola arrasó gran parte de la ciudad de Lisboa así como zonas cercanas, causando entre 10.000 y 100.000 bajas.

En la actualidad, en España se trabaja en un sistema de alerta temprana de terremotos y tsunamis, en el que se deben incluir redes de mareógrafos y estaciones sísmicas, así como de receptores GPS operados de forma continua (CGPS), complementando a los sismómetros tradicionales. Esto aumentaría la capacidad de detección de eventos potencialmente peligrosos.

Objetivos de la Investigación

Este trabajo se centra en la Península Ibérica. Aprovechando estaciones GPS previamente establecidas y de uso público, más las propias del Real Instituto y Observatorio de la Armada (ROA), se estudia el movimiento de dichas estaciones en tiempo casi real mediante un procedimiento ininterrumpido adecuado a tal finalidad.

Para ello, se procesan datos GPS recogidos cada segundo por una red de estaciones en la zona de estudio y se investiga el movimiento relativo entre las estaciones en diversos casos de prueba.

El programa usado para el tratamiento de tales registros es Bernese v. 5.0 (desarrollado en la universidad de Berna, Suiza). Las estaciones seleccionadas son de los organismos internacionales IGS y EUREF así como del ROA, poniendo especial interés en estas últimas (SFER, ALBO, VELE, ROAP y ROTA). Además, las estaciones de la red Meristemum (región de Murcia) se usan para el ejemplo principal.

Caso de Prueba

Se usan los datos de diferentes estaciones sísmicas y GPS obtenidos durante el pasado terremoto de Lorca (Murcia) en mayo de 2011. Tras el procesamiento de la información de los GPS, se comparan con los registros sísmicos, pudiendo así comprobar la sensibilidad del procedimiento creado para el proyecto.

Resumen

Los receptores sísmicos se saturan cuando la intensidad de un terremoto es media-alta. Por tanto, es a partir de ese rango cuando un receptor GPS puede ser útil complementando a aquellos, ya que un GPS es capaz de medir desplazamientos (tanto horizontales como en la vertical) sin saturarse. Por tanto, una red de receptores GPS es un método más que adecuado para una rápida determinación de la localización de un seísmo y una primera estimación de su magnitud.

Con la finalidad de crear un sistema de alerta temprana, es importante conseguir un procesamiento rápido: la red de estaciones debe ser capaz de identificar la magnitud de cualquier seísmo de intensidad media-alta ocurrido en la Península en el menor tiempo posible. Con tal evaluación, una alerta temprana podría ser enviada a los organismos pertinentes para tomar de inmediato las medidas oportunas.

Después de detectarse un movimiento anómalo, su registro se compararía con una base de datos que incluyese casos extremos obteniéndose una estimación real del peligro al que se estaría expuesto. Entre las posibles aplicaciones de este estudio se encuentra la determinación de la magnitud de un evento a partir del movimiento del suelo, teniendo en cuenta la cercanía al epicentro y la dirección de ruptura del terremoto, entre otros factores.

Chapter 1

Introduction

On May 11th, 2011, 16:47 UTC, a M_W 5.1 magnitude earthquake occurred near the town of Lorca (Murcia, Spain) [IGN, 2011]. The reported location of the epicenter was only about 2 km East-Northeast of the city (37.699^{o}N, -1.673^{o}W), with a hypocentral depth of only about 3 km, as stated in [Cabañas-Rodríguez et al., 2011]. Lorca is placed in the Eastern Betics Shear Zone, a region that has suffered a significant number of moderate-to-large magnitude earthquakes in the past 500 years. It is considered one of the areas of highest seismic risk in Spain. According to [López-Comino et al., 2012], the locations of the 149 events within the earthquake sequence show no discernible pattern. However, detailed seismic relocation leads to the Alhama de Murcia Fault as the generator [López-Comino et al., 2012].

In this region, the GNSS network "Meristemum" [http://gps.medioambiente.carm.es/] is deployed, including six stations (see Table 1.1 and Figure 1.2) and providing 1 Hertz observations.

Station	**STATION NAME**	**Epicentral Distance (Km)**
LORC	Lorca	5
CRVC	Caravaca de la Cruz	49
MURC	Murcia	58
CRTG	Cartagena	62
SALI	San Pedro del Pinatar	80
JUMI	Jumilla	91

Table 1.1: Considered stations from Meristemum GPS network.

The analysis of data recorded from the aforementioned network (see Figure 1.2) is achieved in this project. Such stations are included in a custom network called Topo, using GNSS receivers from EUREF, IGS and ROA (Figure 1.1) which are deployed in the Iberian Peninsula and its surroundings. Using "Bernese v. 5.0" software, a kinematic Double Differences (DD) analysis of the data is performed and the detection of the earthquake signal within the time series from Meristemum stations is achieved.

A first evaluation of the observation data from station LORC (the closest from the epicenter, see Table 1.1) shows that some periodical oscillations with peak-to-peak amplitudes of $\sim$2 centimeters in the North-South (N-S) direction are detected in a timespan of 20 seconds, as shown in Figure 1.3. In the same figure, but for the East-West (E-W) direction as well as in height, displacement with peak-to-peak amplitudes up to a centimeter are clear.

To work out the effect of the influence from seismic waves on the station positions, an attenuation method is applied: the so-called Modified Sidereal Filter (MSF). It removes most of the periodic influence (temporal correlation) due to the satellite constellation recurrence,

and especially multipath effects. An event can be identified without applying such attenuation methods, but the real amplitude of the movement can be obtained after improving the data.

The five remaining stations in the network were processed as well and found stable. Their distance to the hypocenter seems to be too long to get any discernible motion above noise level. This result is in agreement with [Gonzalez et al., 2012].

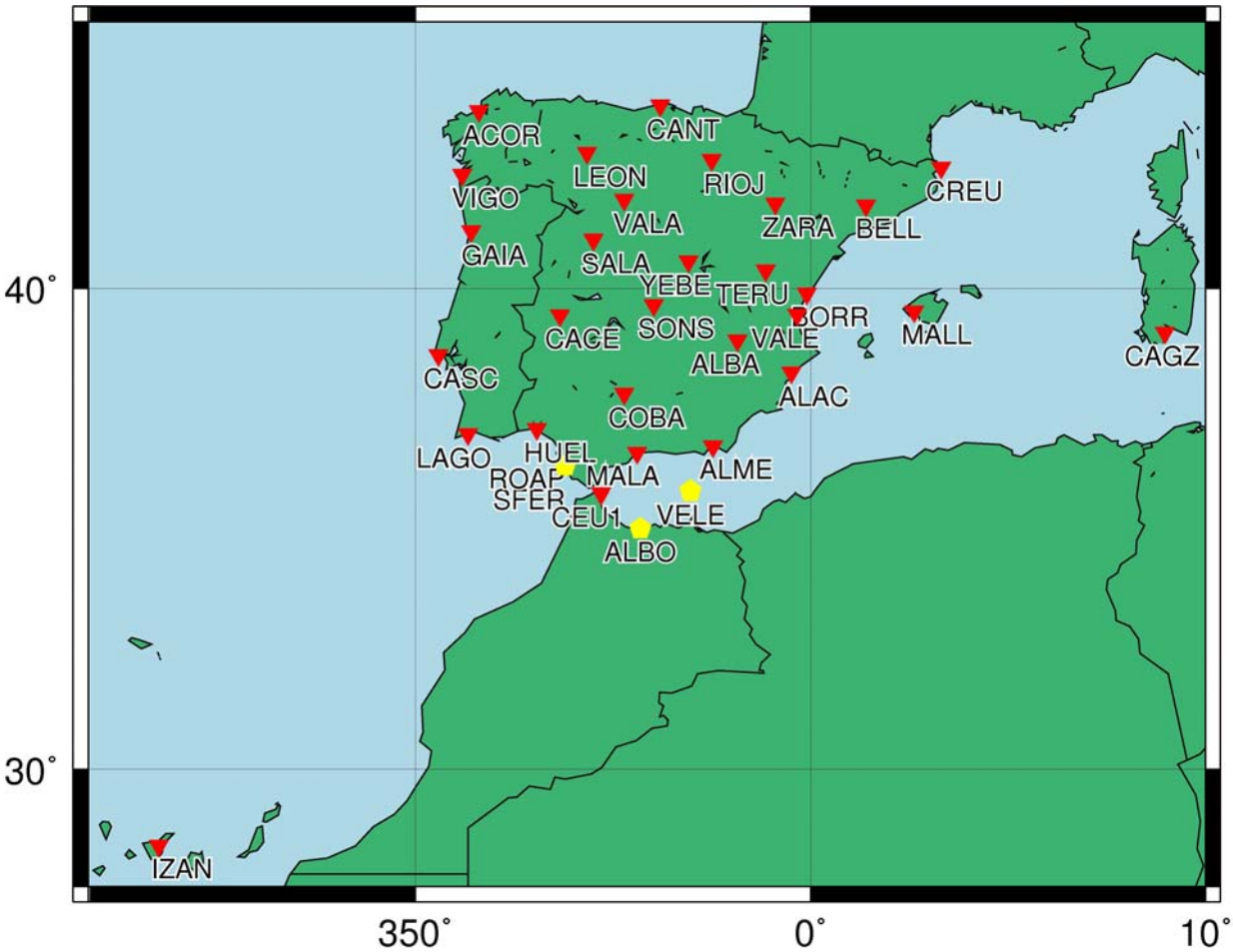

Figure 1.1: GPS Stations from Topo network. Red triangles: EUREF and IGS stations. Yellow dots: ROA stations.

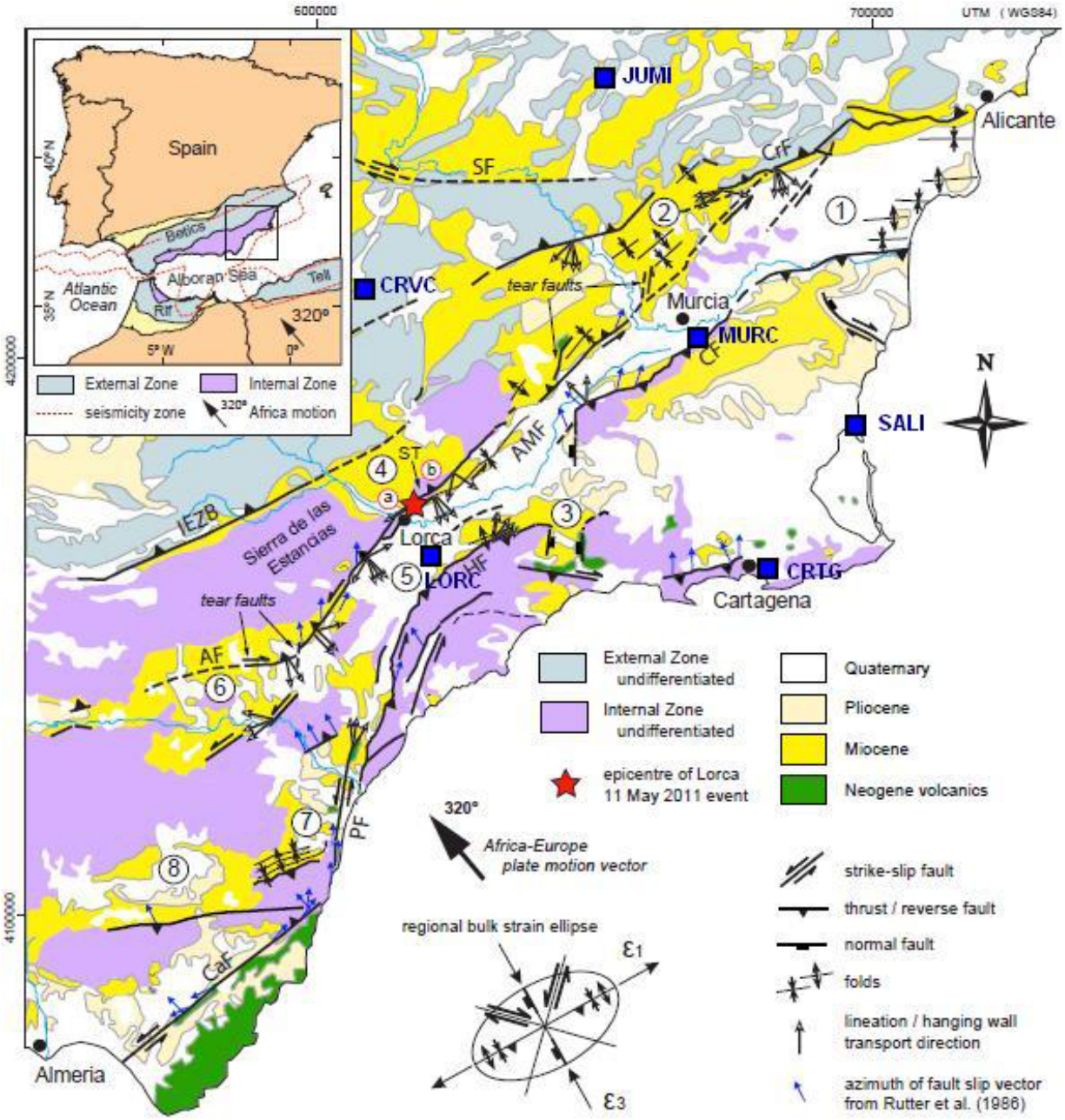

Figure 1.2: Meristemum network map, GPS stations marked as blue squares. Murcia Province tectonic settings. Map modified from [Vissers and Meijninger, 2011].

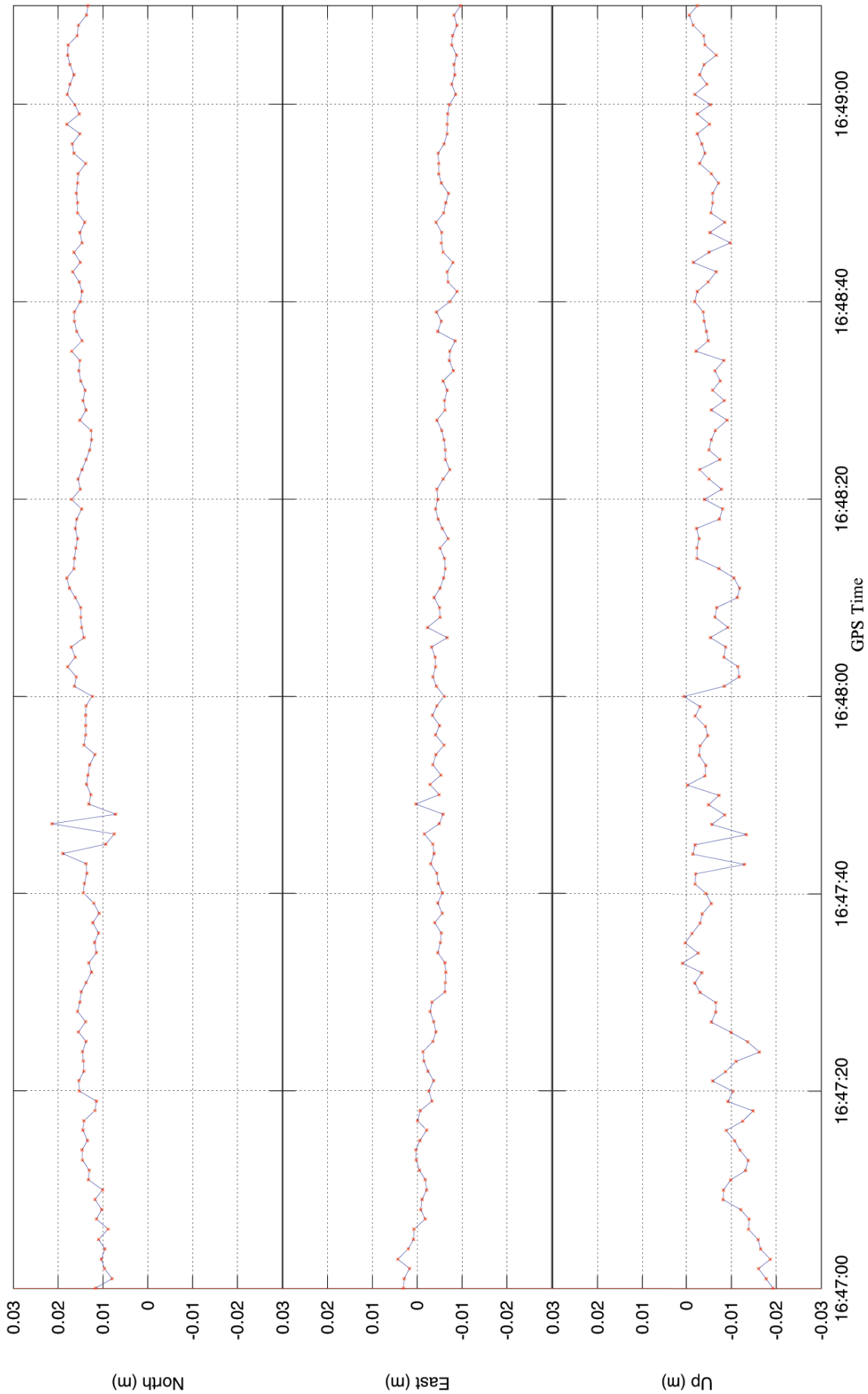

Figure 1.3: Time series for station LORC at the time of the earthquake (16:47:42 GPST). Unfiltered results, obtained from Double Differencing.

Chapter 2

Processing

Selected stations time-dependent positions are analyzed, and the variations in their coordinates are determined by using a baseline processing or Double Differencing (DD). After this, residuals are processed by the so-called Modified Sidereal Filtering (MSF), improving the results after filtering. Software modules for MSF and other data processing are created with the help of Perl and Matlab software packages.

The data analysis is carried out using Bernese v. 5.0 software. This geodetic tool was developed at Bern University, Switzerland. It can process the two currently active GNSS systems (American GPS and Russian GLONASS).

Bernese v. 5.0 can be customized for the users needs due to its modular design, also being able to run multi-sessions in parallel. It processes both Double Differences and Precise Point Positioning (PPP) strategies, being capable of accomplishing a kinematic analysis as well.

Bernese Processing Engine (BPE) is used for the GPS data analysis. BPE is a tool that runs Bernese in a fully automatic mode. Individual scripts are accurately determined and processed, allowing for a much faster analysis of the data.

The entire analysis can be divided into three sections: download of the data, processing with Bernese and documentation of the results, and preparation of the residuals. An extra section is incorporated, detailing the automation implemented (Section 2.3).

2.1 Data Provision

Before starting with the analysis, preparations must be made. Necessary data is obtained from the on-line services provided by different organizations, and later used in the processing. Observation files are downloaded as well as available orbit and ERP data files.

2.1.1 Monitoring Data

For a normal kinematic near-real time processing, RINEX observation files are downloaded, with 15 minutes latency and 1-Hz sampling rate, from the corresponding FTP servers at ROA, IGS, EUREF, or other FTP sites when necessary (see Chapter 6).

2.1.2 Orbit Data

For near-real time processing, IGS Ultra-Rapid products are fetched from [ftp://cddis.gsfc.nasa.gov/gps/products/WWWW], where WWWW is the corresponding GPSWeek.

The repetition rate (or Aspect Repeat Time, ART, see Section 2.4.2) calculation requires precise orbital data (precise IGS SP3). This can be directly downloaded from the IGS website [http://igscb.jpl.nasa.gov/components/prods_cb.html]. Unfortunately, such data is not available for near-real time processing.

2.1.3 Other Data

From CODE database [ftp://ftp.unibe.ch/aiub/CODE], ionospheric information for each day is also downloaded.

2.2 Data Evaluation and Documentation

Evaluation strategy and observation interval as well as the reference station selection must be ascertained for the process. Once achieved, two steps are needed in order to determine subdaily movement for each station, like tectonic displacement for example. First, static coordinates are estimated by the program GPSEST, using atmospherical parameters and fixing ambiguities. After that, a further GPSEST run provides the kinematic analysis. And, in the end, a perl script stores the estimated kinematic coordinates into a new plain text file for each station.

2.2.1 Bernese Setup. Data Organization and Storage

Before running Bernese software, eight folders are created: ATM, BPE, OBS, ORB, ORX, OUT, RAW, SOL and STA. Some of them are empty until the process starts. Those that must be filled are: ATM, where Ionosphere and Troposphere files are downloaded; ORB, enclosing Pole and Orbit files; RINEX data packages are sent to ORX; and STA contains all the station information needed, this is:

- A coordinate file (*.CRD) including the station's coordinates in a geocentric reference system.
- A station abbreviation file (*.ABB) defining two- and four-character abbreviations for the stations[1].
- A station information file (*.STA) containing receivers and antennas information, as well as the eccentricity of the latter. It also details changes in the station's equipment.
- A tectonic plate information file (*.PLD) describing the tectonic plate in which each station is located.

2.2.2 Preprocessing

Every 15 minutes, a file is downloaded for each station, containing 1 Hz GPS observations for the last 15 minutes. Such observation files in RINEX format are joined into 6-hours packs[2], because it is mandatory to process's more than 6 hours of data in order to obtain a suitable ambiguity resolution. The aforementioned packages are then transformed into Bernese binary format and imported to the correspondent folder (/RAW). This is achieved through the programs CCRNXO and RXOBVE, respectively.

After that, CODSPP synchronizes the receiver clocks with GPS time and determines approximated station coordinates using zero-difference measurements. It derives ionosphere

[1] An example of four-character abbreviations can be seen in Table 1.1.

[2] Therefore, running the whole process must take less than 15 minutes, to avoid overlapping with the following.

free code observations and stores the results into the phase observation files. Four different files in binary Bernese format are obtained:

/*.CZH: Code Observation / zero difference / header file

/*.CZO: Code Observation / zero difference / observations

/*.PZH: Phase Observation / zero difference / header file

/*.PZO: Phase Observation / zero difference / observations

Polar motion information is transformed into Bernese format. Orbital data also needs to be processed before its information is integrated into the subsequent steps. For that reason, conventional orbit information is converted into tabular orbits (*.TAB) and clock files (*.CLK) by PRETAB. Obtained tabular orbits in addition to the pole motion data are the bases for the standard orbits (*.STD) generation.

In the following step, single-difference baselines are formed for each session by SNGDIF. Optimal results, in terms of ambiguities resolved ratio, are reached when baselines are defined by the maximum number of observations between two stations. Therefore, since automatic procedure depends on the data available, baselines set change every 15 minutes, directly preventing continuity for the resulting time series. For this reason, in this project baselines are fixed and the selection strategy will be explained in Section 6.3. This procedure of single differencing eliminates the receiver clock error terms in the model[3]. Tropospheric and ionospheric effects are also reduced through single differencing, especially for those stations close from each other. Single-point absolute positioning is generated by only code measurements. To form the single-phase baselines, just phase-based differences are taken.

The last subprogram for pre-processing is MAUPRP, consisting in the search and elimination of cycle slips. Finding cycle slips formed during single differencing allows further determination or even the elimination of such ambiguities. In addition to the data cleaning process, this step can be used to determine a first float coordinate solution.

Static Coordinates Calculation

In order to obtain kinematic coordinates, good previous static coordinates must be fixed, as well as atmospheric parameters. In the first run of GPSEST subprogram, residuals of the coordinates based on Double Differences are estimated according to the standard proceeding, as explained in [Beutler et al., 2008]. In this step, an ionosphere-free linear combination (L3) is used. SATMRK marks the inconsistent residuals in the residual data file so they are not used in further processing. This is, a first order ionosphere-free equation is formed with unknown ambiguities.

In a following step, ambiguities are fixed. The resolution strategy depends on the length of the baseline considered:

- Short-Lane strategy is used for baselines up to 50 km.
- Widelane-Narrowlane is used for baselines from 50 to 200 km.
- QIF strategy is used for baselines longer than 200 km.

For each session, the solution is found by fixing the ambiguities in the static coordinates, which are later used as apriori coordinates. Troposphere parameters are also needed during kinematic processing, thus are calculated as well.

[3]However, the satellite clock error, which implicitly affects computation of satellite and station positions, is yet to be carefully considered.

2.2.3 Kinematic Analysis

In the end, a kinematic processing is carried out for the last 15 minutes data and for one of the stations in each baseline. By convenience, the station considered as fixed is the first in the baseline, and the last is treated as kinematic. The evaluation is performed as a ionosphere-free combination with fixed (known) ambiguities. If baselines are short, tropospheric parameters are very similar for each station in the baseline, but for longer baselines, such parameters must be considered. They are taken from the last 6 hours of output data.

2.2.4 Documentation of the Results

Resulting kinematic coordinates are extracted from Bernese output and saved in a suitable format for further processing. This is, GPSEST output written in OUT/*.OUT is read by a Perl script. Kinematic coordinates are then stored in a text file, in columns: the first one shows the epoch of the residual (in MJD); and the second, third and fourth columns correspond to the residuals in North, East and height (in meters), respectively. An example is found in Figure 2.1.

55694.020845	-0.0022	0.0226	-0.0398
55694.020856	0.0007	0.0252	-0.0340
55694.020868	-0.0019	0.0241	-0.0350
55694.020880	-0.0044	0.0241	-0.0395
55694.020891	0.0012	0.0253	-0.0385
55694.020903	-0.0018	0.0239	-0.0454
55694.020914	0.0029	0.0248	-0.0405
55694.020926	0.0005	0.0235	-0.0401
55694.020938	0.0023	0.0257	-0.0399
55694.020949	0.0017	0.0239	-0.0356
55694.020961	0.0016	0.0270	-0.0374
55694.020972	-0.0029	0.0270	-0.0303
55694.020984	-0.0046	0.0247	-0.0324
55694.020995	-0.0043	0.0246	-0.0410
55694.021007	-0.0006	0.0271	-0.0377
55694.021019	-0.0019	0.0252	-0.0453
55694.021030	0.0004	0.0213	-0.0447
55694.021042	0.0003	0.0218	-0.0387

Figure 2.1: Extract from kinematic coordinates storage for station CRVC. First column indicates the date in GPST. Second, third and fourth, the residuals, in North, East and height, respectively.

GPSEST output is named YYDOY_15.OUT[4] and stored in a folder with self-explanatory name, pointing to the correspondent 15 minutes gap: YYYY/DOY/H/GPSDATA_MM where H is the hour in letter (A, B, ..., X) and MM the minute (00, 15, 30 or 45[5]. The kinematic output file is stored in two places, one of them in the same folder under the name YYDOYHMM.KIN, and the other appended to a file containing kinematic coordinates for the day being processed, YYYY/DOY/DOY.KIN.

2.3 Automatic Processing

GPS receivers are prepared to measure a very large amount of data during surveys that can last weeks or even months, and such volume of data clearly demands an automated analysis. Bernese software can execute all possible tasks in batch mode or in parallel, and

[4]Example 11232_15.OUT, year 2011, DOY 232, 15 minutes solution.
[5]Example 2011/232/C/GPSDATA_15, year 2011, DOY 232, 2 a.m., data from minute 15:00 to minute 29:59.

its evaluation procedure can be defined by the so-called "Process Control Files" (PCFs), establishing waiting rules when necessary.

2.3.1 Parallelization

The objective of parallelization is shortening the processing length. CCRNXO, MAUPRP, CODSPP and GPSEST are the subprograms related to baseline or single station processing, this is, for each baseline or station, the aforementioned scripts must run once. Hence, as long as the computer has more than one core, parallelization allows the processes to run at the same time without overlapping, one baseline or station for each computer core.

Time saved by parallelizing the aforementioned subprograms depends on the number of stations to be processed and the number of cores available. For this example, 6 hours of data from a set of 30 stations is processed in a computer with two processors and 8 cores. Up to five minutes can be saved by the parallelization of CCRNXO, and MAUPRP run is shortened one minute. When testing CODSPP, the time reduction goes up to a minute. Parallelization of GPSEST gives the maximum time reduction in the process: short, medium and long baselines run in parallel, saving up to 7 minutes for a 6 hours data processing.

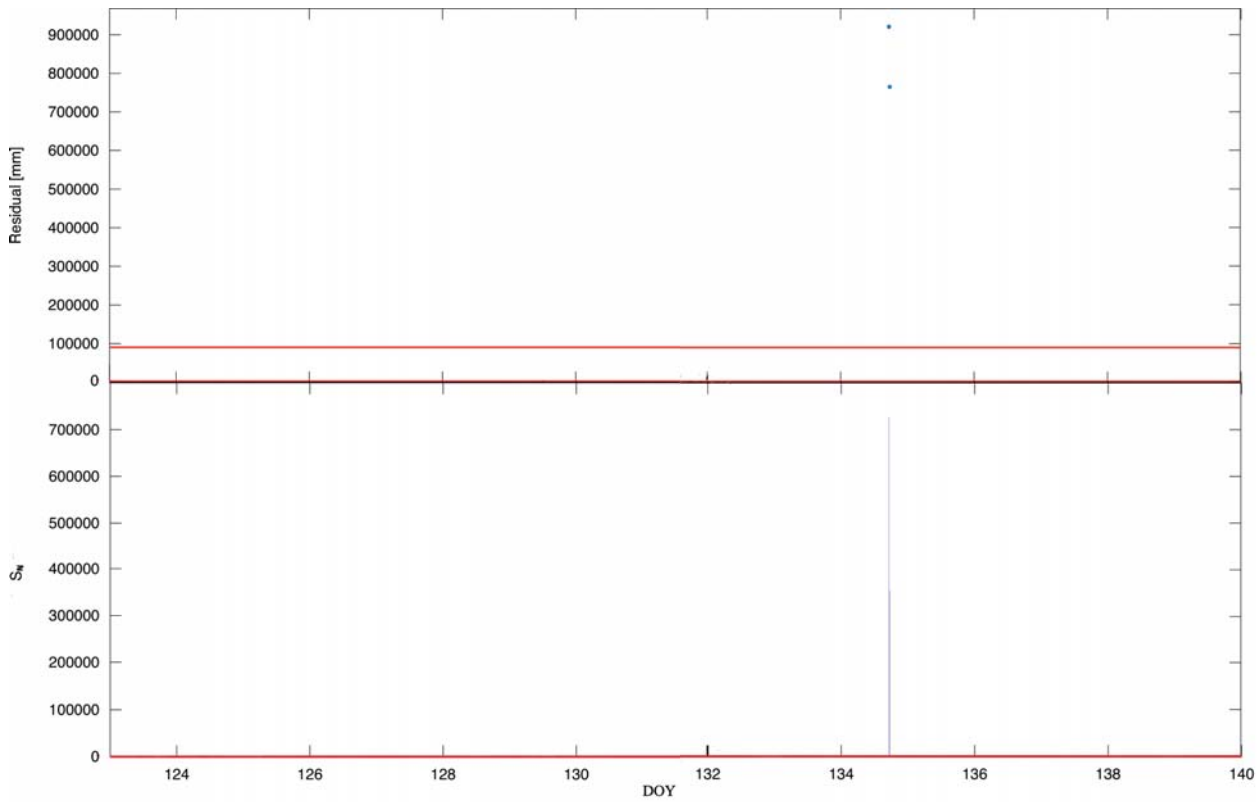

Figure 2.2: LORC unscreened time series. Residuals for DOY 123 to 140 are plotted (above) as well as their empirical sigma (below). Two outlying residuals are clearly visible for DOY 134 (blue dots). Horizontal red lines define 3IQR[7]. Due to the outlimited value of both residuals and their empirical standard deviation, the plot scale makes impossible the discernibility of the time series.

[7] A very common screening method is the elimination of results outside 3IQR (3 times Interquartile Range): [mean - 3*S_N, mean + 3*S_N], corresponding to a 95% confidence interval. This approach is not used in this project as explained in Section 5.3.

2.4 Residuals Preparation

Kinematic coordinates are screened and adjusted. Outliers are eliminated when possible, according to a maximum allowable dispersion estimator. The data remaining is demeaned and the blanks in the series are filled in with zeros. Finally, if depending on the satellite configuration, the data is corrected by a Modified Sidereal Filter (MSF).

2.4.1 Results Screening

Time series built directly from Bernese output are shown graphically. In the plots, outliers in the residuals are easily detected, some of them over tens of centimeters (see Figure 2.2). Such large residuals lead to great uncertainties and errors. Therefore, they must be removed.

In order to eliminate outliers, an easy approach consists of finding epochs with very big residuals. Setting the limits for such residuals is the main problem to face. A possible alternative consists of using the kinematic coordinate file and the residuals RMS. According to the fact that residuals are related to the RMS, timespans with excessively large or unreal residuals can be found by screening the data RMS. The problem arising is that, when the mean value of the data is not close to zero, RMS value can be over- or underestimated. Therefore, dispersion estimator Sigma (empirical standard deviation S_N for a sample in the dataset) has to be used.

2.4.2 Modified Sidereal Filter

The accuracy of GPS positioning for a single period can be improved by the reduction of multipath. Multipath effects depend on the instantaneous satellite constellation: each epoch the satellites repeat their aspect with respect to a GPS receiver, multipath repeats its value as well. The GPS satellite constellation at a specific location repeats at intervals of approximately one sidereal day (ideally, 236 seconds less). A Modified Sidereal Filter is based on the period of the satellite constellation (Aspect Repeat Time, ART [Agnew and Larson, 2007]), that is the time a satellite needs in an earth-fixed reference frame to return to a position of minimal distance to the starting position (i.e. same azimuth and elevation). ART varies for each satellite and each station.

Using ASPREP[8] software package [Agnew and Larson, 2007], each satellite repetition rate is calculated. Then, the mean value of such a repetition rate is obtained, using every satellite available. Satellite constellation period is calculated as the arithmetic mean of the individual satellite periods, and its value is rounded to an integer number of seconds.

Applying ASPREP to the data recorded during Lorca earthquake, Aspect Repeat Time (T) is 86155 seconds for DOY 123 in year 2011. Consequently, day 123* goes from 00:00:00 to 23:55:55 GPST, and day 122* goes from 00:04:05 to 23:59:59 GPST of DOY 122. The shift in the data from one modified sidereal day to the following is shown in Figures 2.4, 2.5 and 2.6, where coordinates in N-S, E-W and height components respectively for station LORC and days from 129* to 133* of the year 2011 are plotted as an example. By a visual comparison of the days, repetition patterns are evident, mostly in E-W direction (Figure 2.5). The results improvement after filtering can be observed in the Figures and Tables in Section 3.4.

A near-real time MSF approach is applied considering the data from the last three processed days, schematically shown in Figure 2.3: MSF for one station is based on its position

[8] ASPREP program can only read the old SP3 format (SP3a) and currently IGS delivers SP3c data. Therefore, data must be converted from IGS SP3c to SP3a.

time series for the previous three sidereal days. First, the time series last moment is considered as the end of a sidereal day span. Three epochs in intervals of integer multiples of the ART ($t - n * T$) are searched. Afterwards, these corresponding epochs residuals are arithmetically averaged (stacking) and subtracted from the epoch t solution. Note that when solutions with unsatisfactory quality are found (less than 85% of available output data for a day), such a day is not included in the filter.

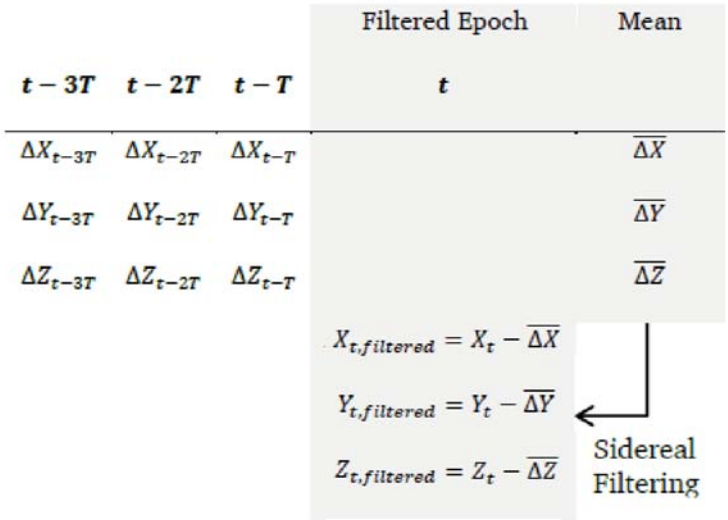

Figure 2.3: Scheme of Modified Sidereal Filter for one station and one epoch.

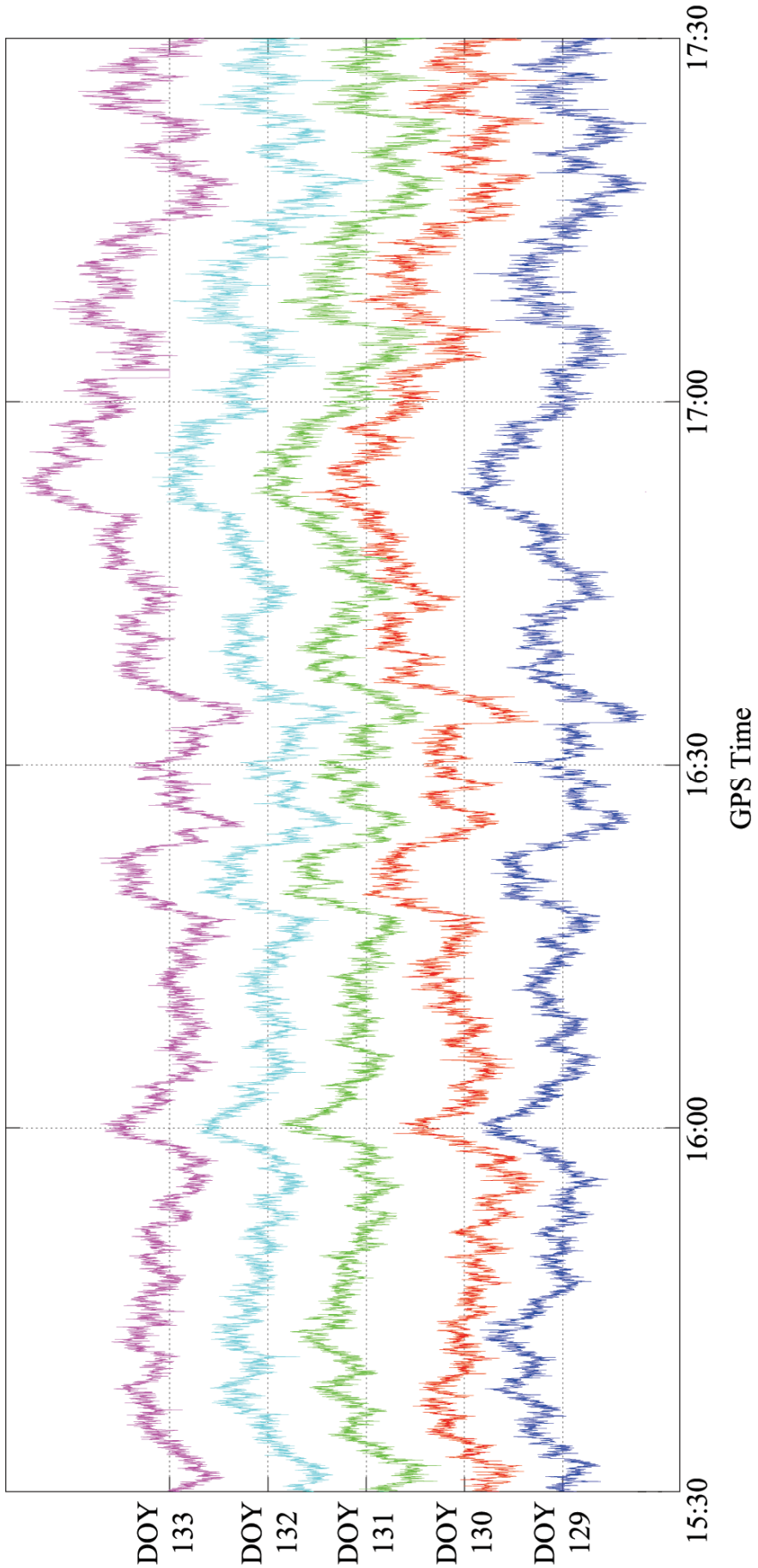

Figure 2.4: Station LORC. Unfiltered North residuals during days 129* to 133* of year 2011. Clear example of the similarities found in the overall behaviour.

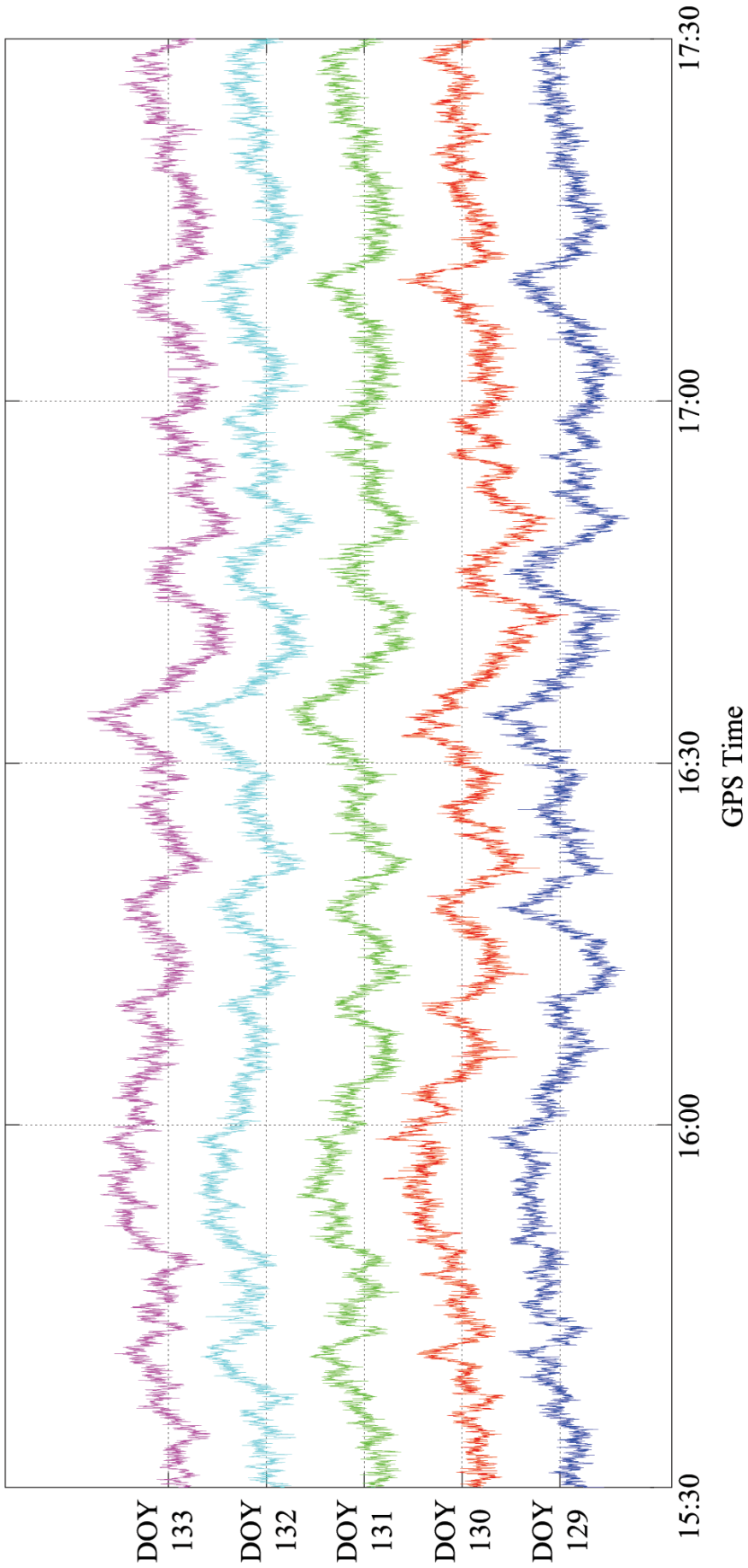

Figure 2.5: Station LORC. Unfiltered East residuals during days 129* to 133* of year 2011. Clear example of the similarities found in the overall behaviour.

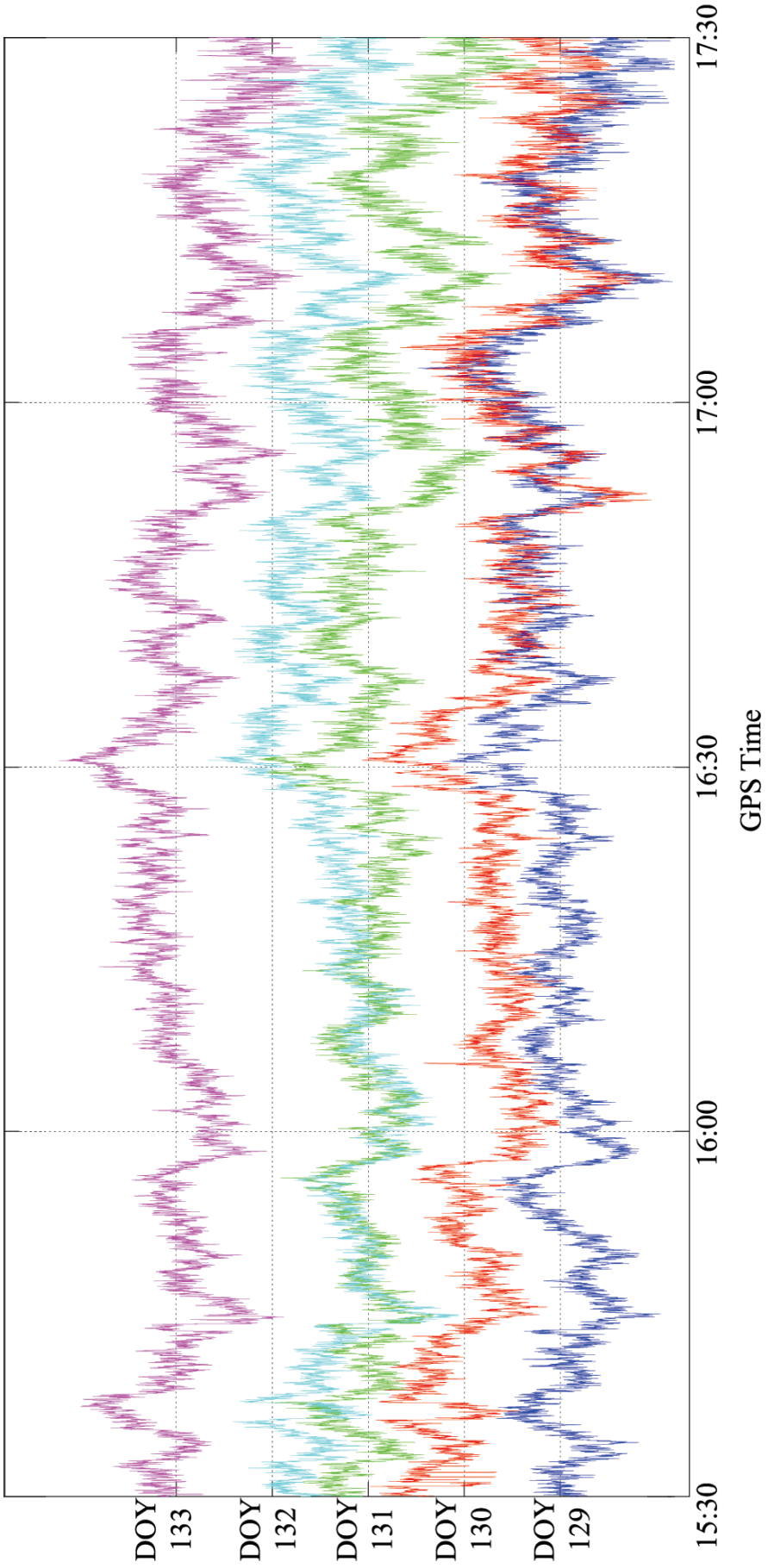

Figure 2.6: Station LORC. Unfiltered height residuals during days 129* to 133* of year 2011. Clear example of the similarities found in the overall behaviour.

Chapter 3

Aposteriori Analysis

Double Differencing approach solutions are shown for two hours of data. MSF is performed for the timespan from 15:30 to 17:30 GPST on May 11th, 2011. A comparison between unfiltered and filtered results is also provided.

3.1 Data Provision

Observation data downloaded for this example is provided by Meristemum network. 1 Hertz RINEX observations of the stations listed in Table 1.1 is available on the FTP server [ftp://meristemum.carm.es/GPS/] in RINEX format. Other data needed is downloaded from IGS and EUREF FTP sites.

To carry out the MSF, all GPS data available for GPSWeek 1635 was downloaded. This week includes the days 128 to 134 in the year 2011. The earthquake occurred at DOY 131. Therefore, the data downloaded corresponds to three days before and after the day to filter.

IGS final products are used for the main analysis. The orbital data in SP3-c format and earth rotation parameters in ERP format were downloaded from the CDDIS FTP server. Such data is also needed to calculate the repetition rate (ART, see Section 2.4.2).

3.2 Ambiguity Fixing Strategy

For the medium-length baselines considered (CRVC-MURC, MURC-LORC, MURC-CRTG, MURC-CRVC, CRVC-JUMI and CRVC-SALI, see Table 6.3 and red lines in Figure 3.1) the best-fit cycle-slip resolution strategy is Widelane-Narrowlane (WL-NL). In every run, each baseline is processed twice. First, ambiguity-free L3 solution is computed, and afterwards, L5 linear combination is processed, and ambiguities are solved. In the second step, the ionosphere-free (L3) linear combination is processed, wide-lane ambiguities are introduced as known and the narrow-lane (L1) ambiguities are solved. In this moment, troposphere parameters estimation is also achieved.

For the purposes in this project, the first station in each baseline is held static and the second is defined as kinematic with 1-meter sigma. Such loose constrain allows the movement of the station within the time series, therefore it can show a displacement whose amplitude could arise up to 2 m.

Baseline	Strategy	% Resolved
CRVC-MURC	WL-NL	96.4
MURC-LORC	WL-NL	89.3
MURC-CRTG	WL-NL	95.6
MURC-CRVC	WL-NL	93.5
CRVC-JUMI	WL-NL	93.3
CRVC-SALI	WL-NL	90.8

Table 3.1: Ambiguity resolution ratio with respect to the baseline considered.

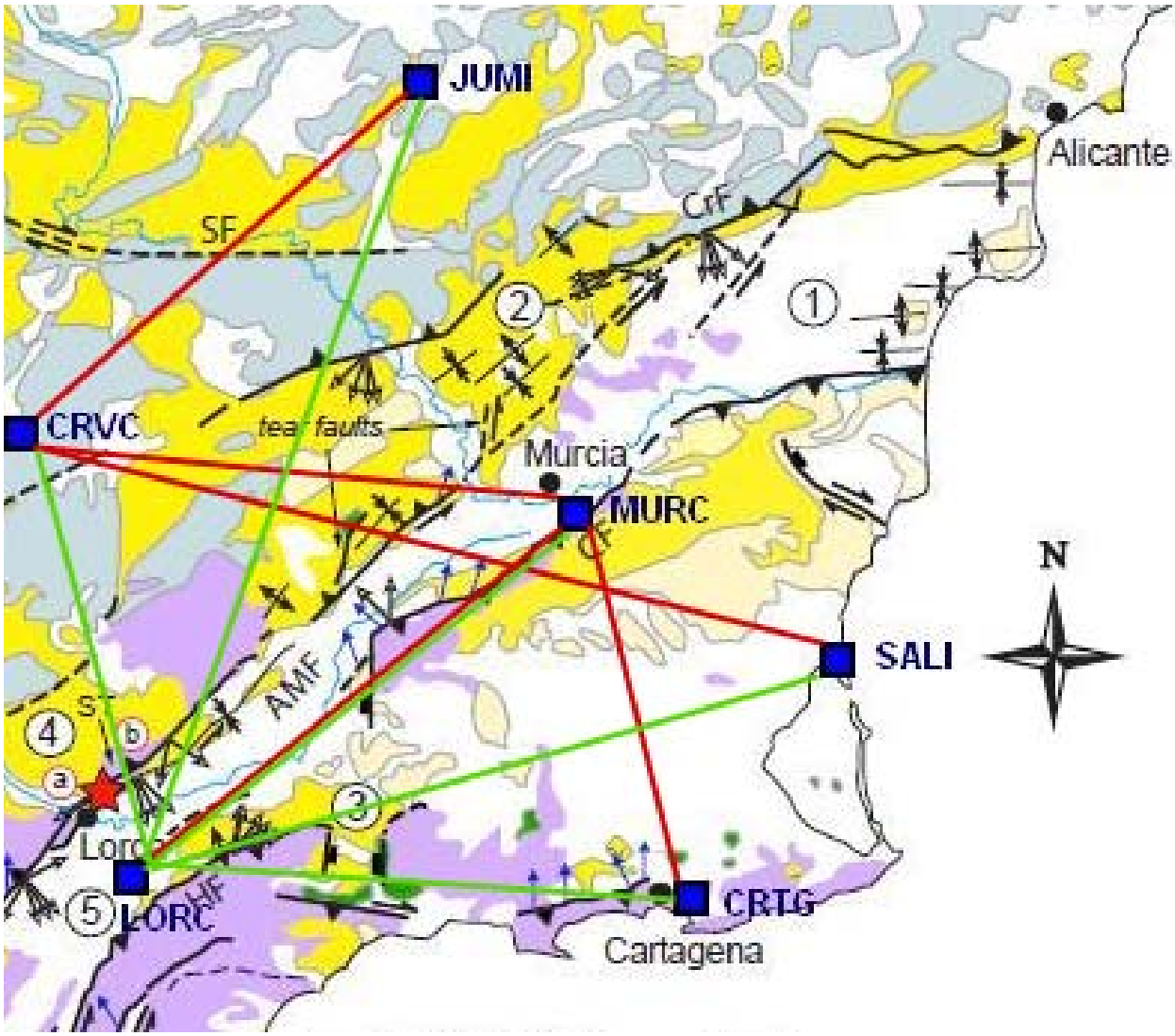

Figure 3.1: Baselines considered in the processing in red. Baselines with station LORC in an edge, in green. Map modified from [Vissers and Meijninger, 2011].

3.3 Modified Sidereal Filter

ART was calculated for a single satellite and reference stations position LORC and MURC, at the reference time DOY 131, 16:47 GPST (the time of the earthquake). The satellite constellation period was calculated as T = 86155 s (rounded to an integer number of seconds). It was the same for both stations.

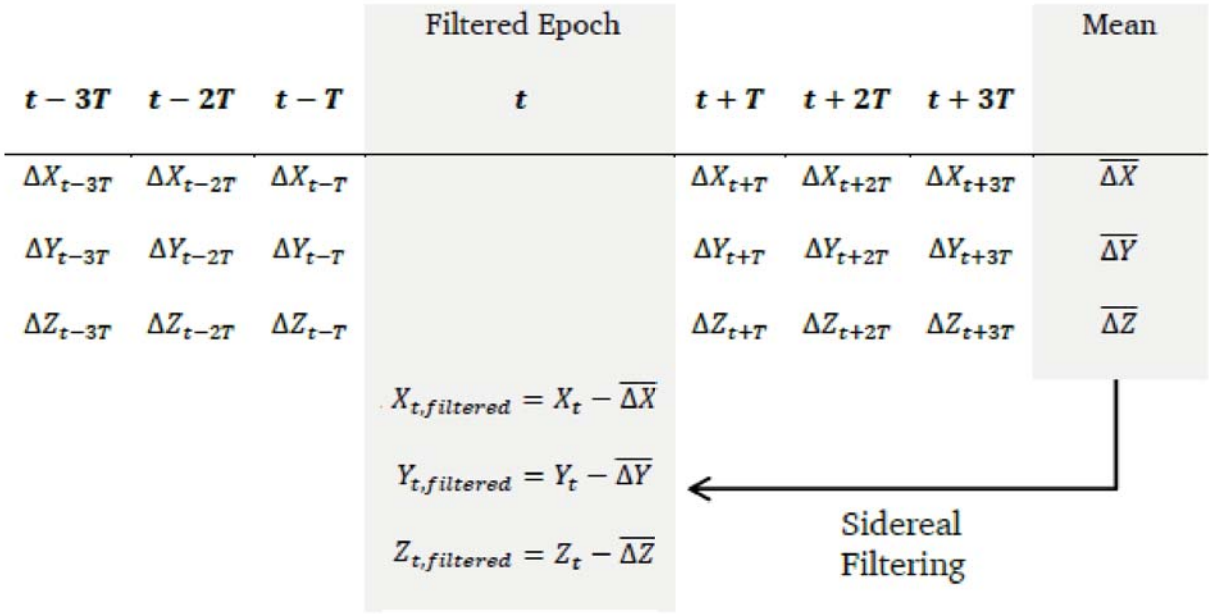

Figure 3.2: MSF scheme for one station and one epoch. Taken from [Mendoza et al., 2012].

Using the advantage that the aposteriori run of the data provides, the sidereal filter is applied here as indicated in Figure 3.2. In this case, MSF for one station is based on its position time series for the whole GPSWeek 1635. The filter setup goes at follows: first, for every epoch t of day 131*, epochs in intervals of integer multiples of the ART ($t \pm n * T$) are searched within GPSWeek 1635; afterwards, each epoch-corresponding residuals are arithmetically averaged (stacking) and subtracted from epoch t residual. As solutions for DOY 134 were found of bad quality, they were not used for this filter.

In Figures 3.3, 3.4 and 3.5, a sidereal filter procedure is shown step by step. First, days of data processed are separated into sidereal days, two days after the event, and three days before it, and their mean value is obtained for each epoch and coordinate. This would be the filter, plotted in pink. After that, such a filter is subtracted from the day to filter (DOY 131, black) and the filtered result smoothness, in red, is clear. Note that all time series plotted are equally scaled.

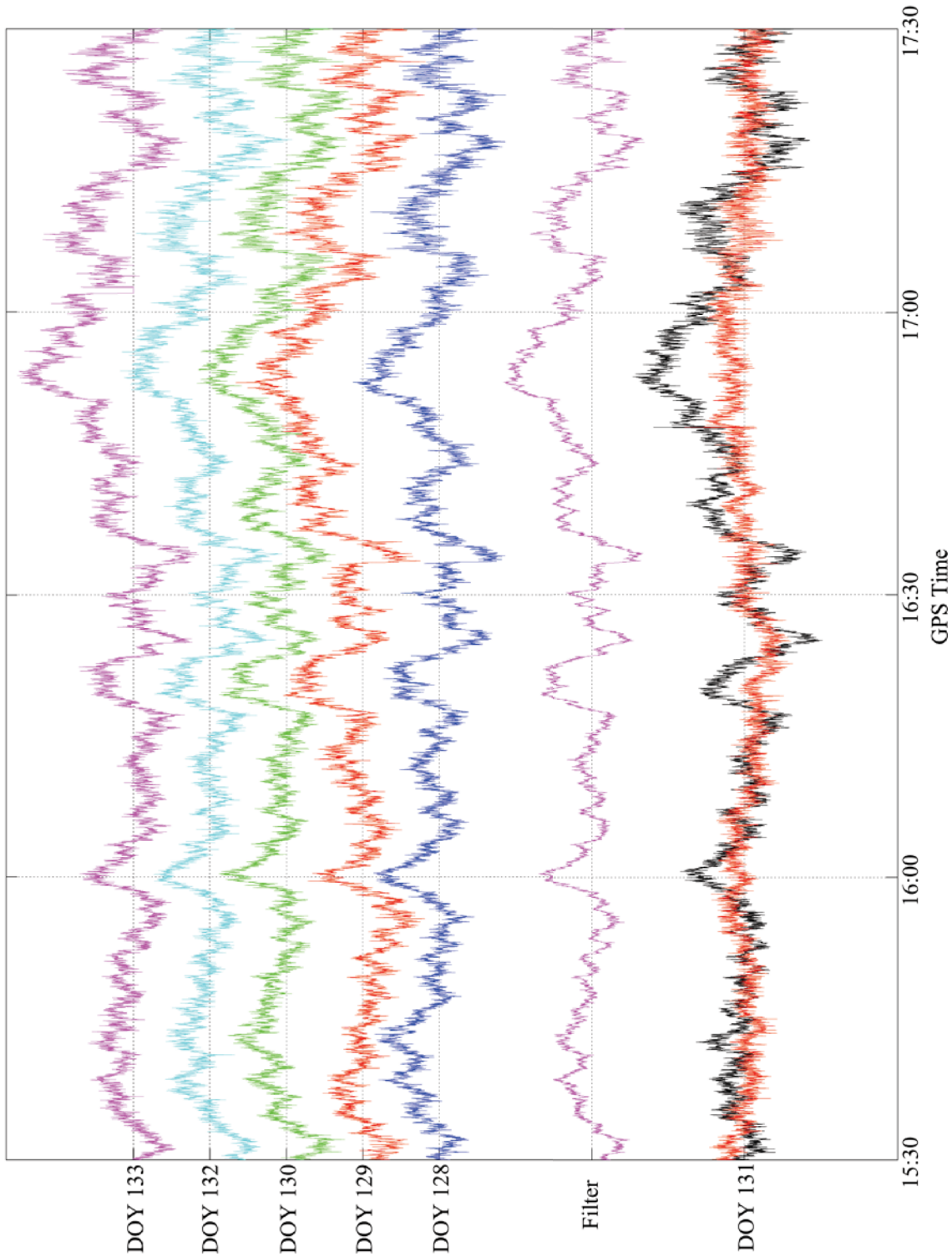

Figure 3.3: Steps for Modified Sidereal Filtering of day 131*. From top to bottom: three days previous and two after the day to be filtered; obtained filter; and raw data from day 131* (in black) and after MSF (in red). North component.

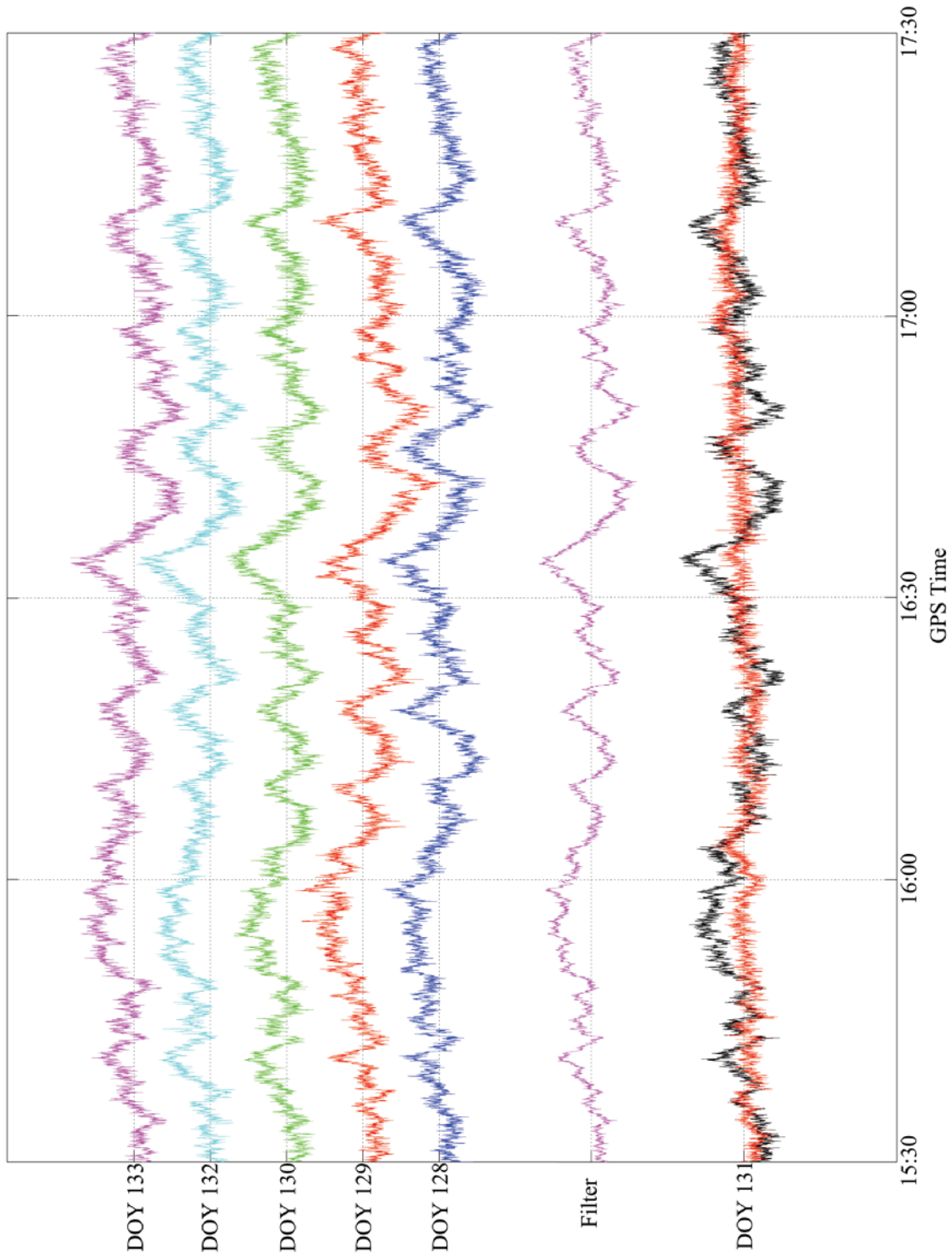

Figure 3.4: Steps for Modified Sidereal Filtering of day 131*. From top to bottom: three days previous and two after the day to be filtered; obtained filter; and raw data from day 131* (in black) and after MSF (in red). East component.

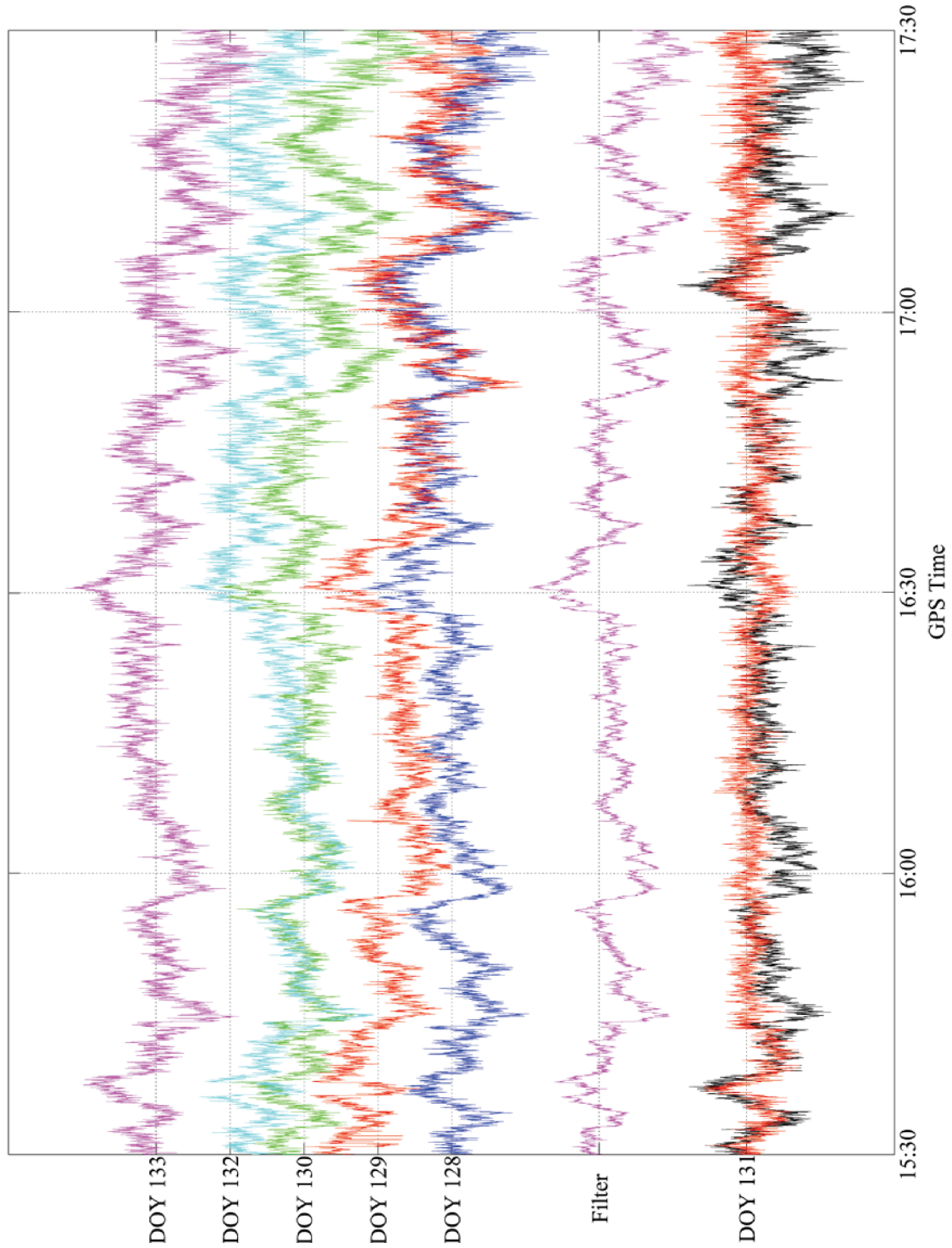

Figure 3.5: Steps for Modified Sidereal Filtering of day 131*. From top to bottom: three days previous and two after the day to be filtered; obtained filter; and raw data from day 131* (in black) and after MSF (in red). Height.

3.4 Summary of the Results

DD results indicate a short-period noise and partially long-periodic fluctuations (for example, DD MURC solutions in Figure 3.7).

Fluctuations are effectively eliminated by sidereal filtering, as one can see by the standard deviation decrease (specially visible in MURC station). However, high-frequency noise is not reduced. The position accuracy after filtering presents a homogeneous reduction in the level of the standard deviation in N-S and E-W, around 43-55%. Moreover, reduction around 30-40% is achieved in height.

		DD Raw	**DD MSF**	**%**
LORC	S_N N-S (mm)	12.0	5.4	**55.0**
	S_N E-W (mm)	7.5	4.3	**42.7**
	S_N Up (mm)	13.6	8.3	**39.0**
MURC	S_N N-S (mm)	11.7	6.0	**48.7**
	S_N E-W (mm)	10.0	5.5	**45.0**
	S_N Up (mm)	14.3	9.9	**30.8**
CRTG	S_N N-S (mm)	11.4	5.6	**50.9**
	S_N E-W (mm)	8.4	5.1	**39.3**
	S_N Up (mm)	16.6	11.6	**30.1**
CRVC	S_N N-S (mm)	11.7	5.9	**49.6**
	S_N E-W (mm)	10.1	5.6	**44.5**
	S_N Up (mm)	14.2	10.2	**29.2**
JUMI	S_N N-S (mm)	10.2	4.5	**55.9**
	S_N E-W (mm)	9.2	4.6	**50.0**
	S_N Up (mm)	21.0	9.9	**52.9**
SALI	S_N N-S (mm)	7.5	5.9	**21.3**
	S_N E-W (mm)	5.7	4.2	**26.3**
	S_N Up (mm)	13.0	10.4	**20.0**

Table 3.2: Empirical standard deviations (S_N) for Meristemum network stations. DD before and after applying MSF. Improvement ratio between unfiltered and filtered solutions. Time interval considered: from 15:30:00 to 17:30:00 GPST.

In the Figures corresponding to the network stations (3.6, 3.7, 3.8, 3.9, 3.10 and 3.11) the improvement in the time series is also visible, as well as in Table 3.2. Data is less scattered and the standard deviation reduction is indicated in the legend. This is due to the periodicity in the data used, clear in Figure 2.5 for East component in station MURC.

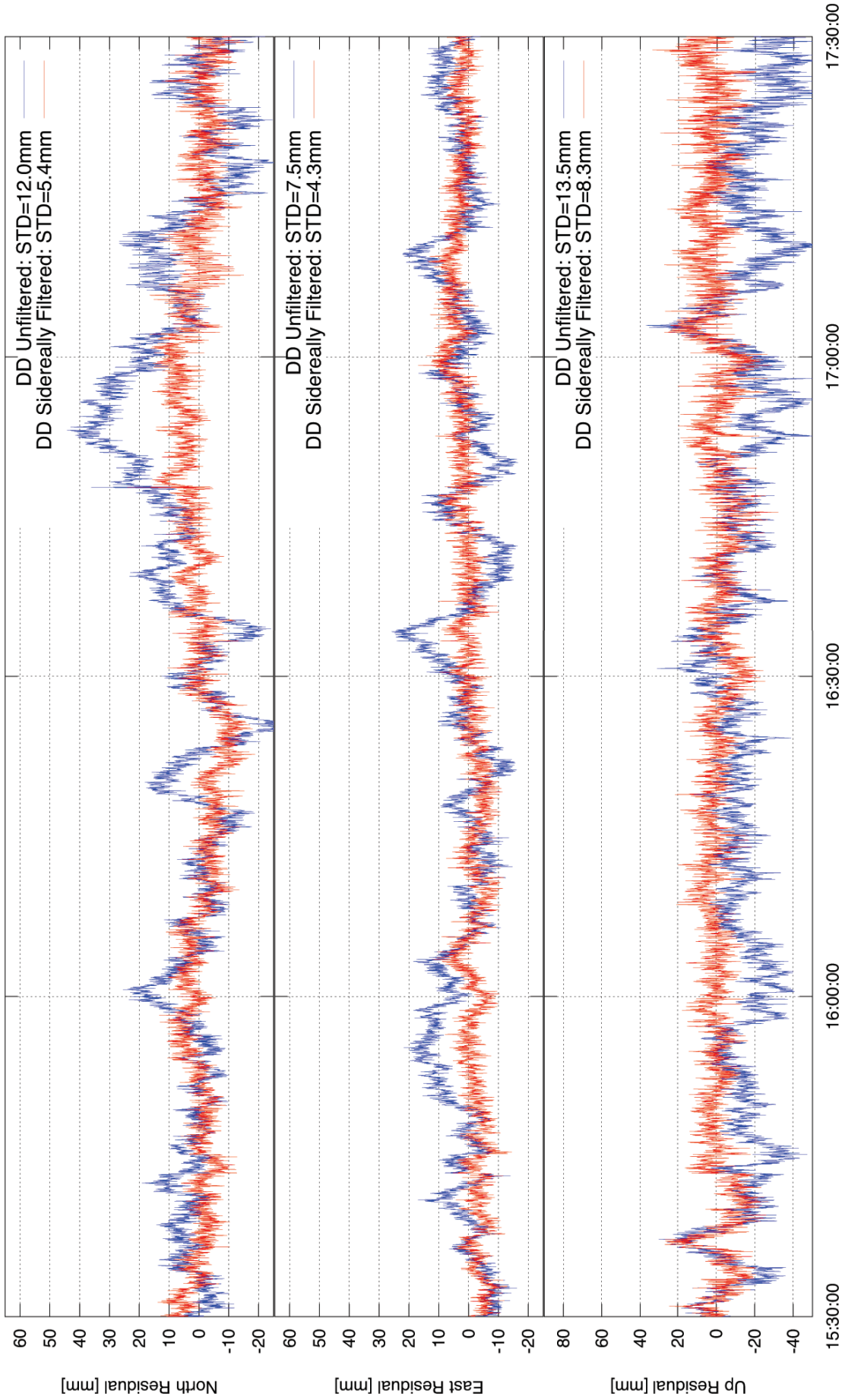

Figure 3.6: Time series for station LORC, unfiltered (blue) and filtered (red) for DOY 131.

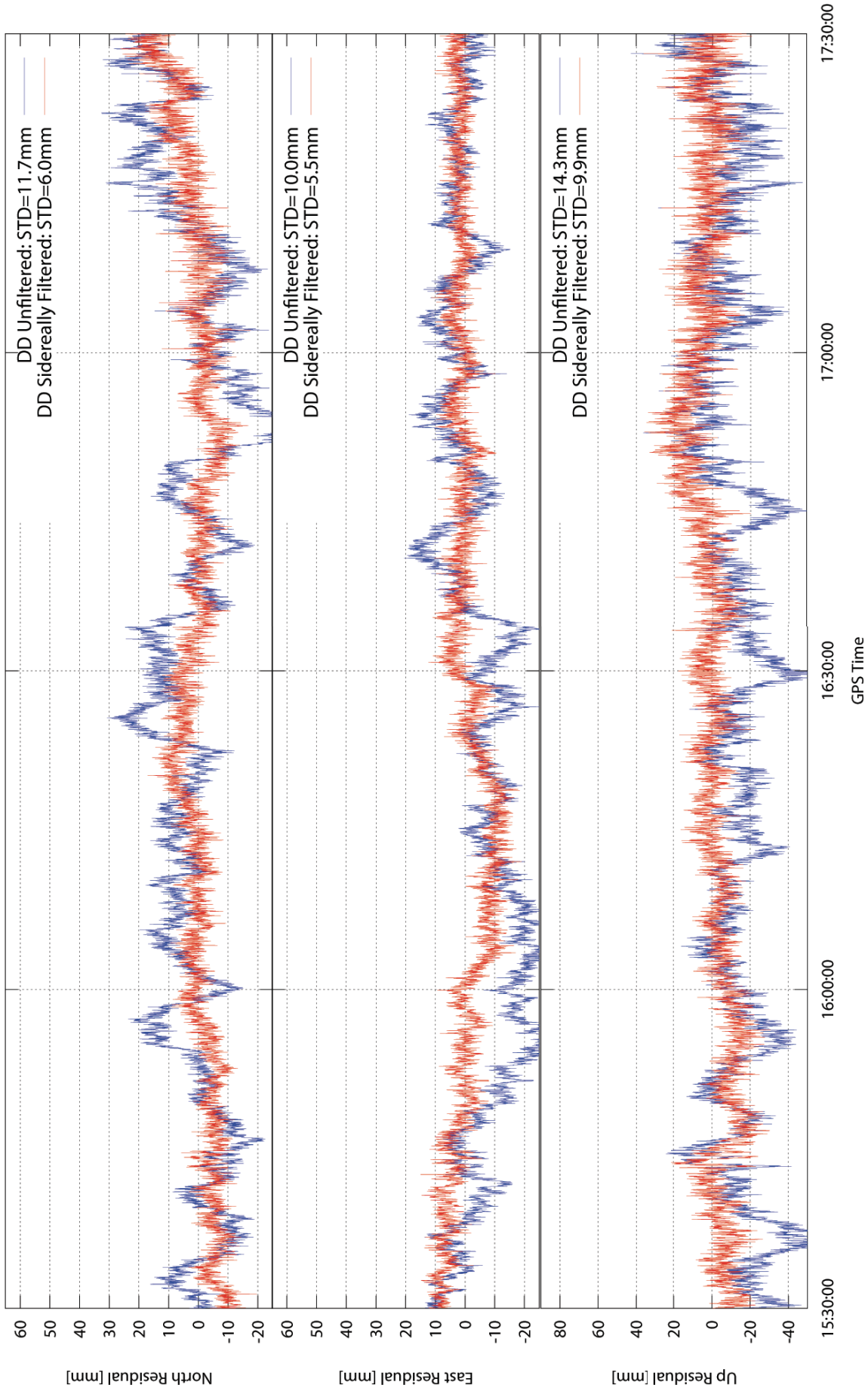

Figure 3.7: Time series for station MURC, unfiltered (blue) and filtered (red) for DOY 131.

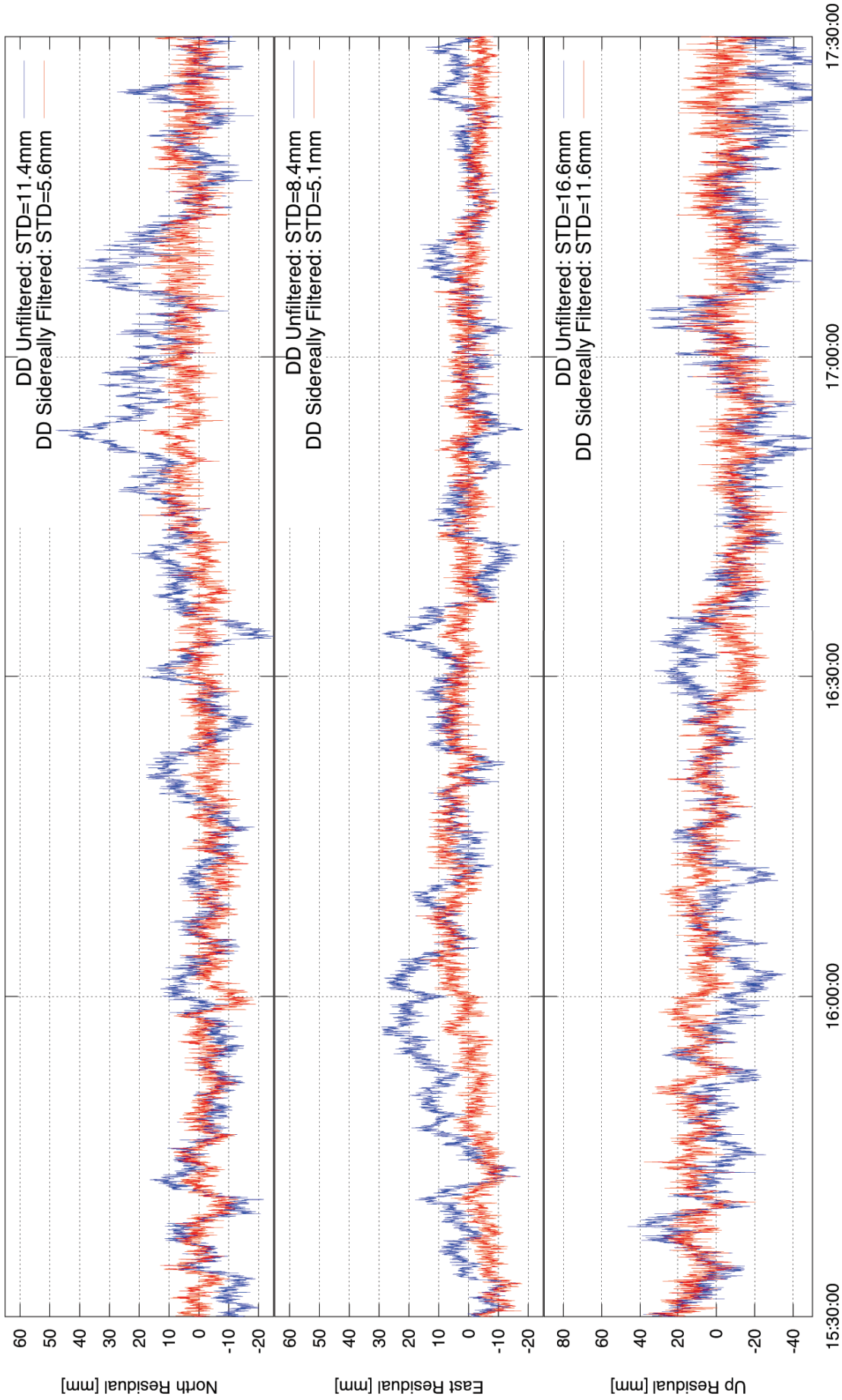

Figure 3.8: Time series for station CRTG, unfiltered (blue) and filtered (red) for DOY 131.

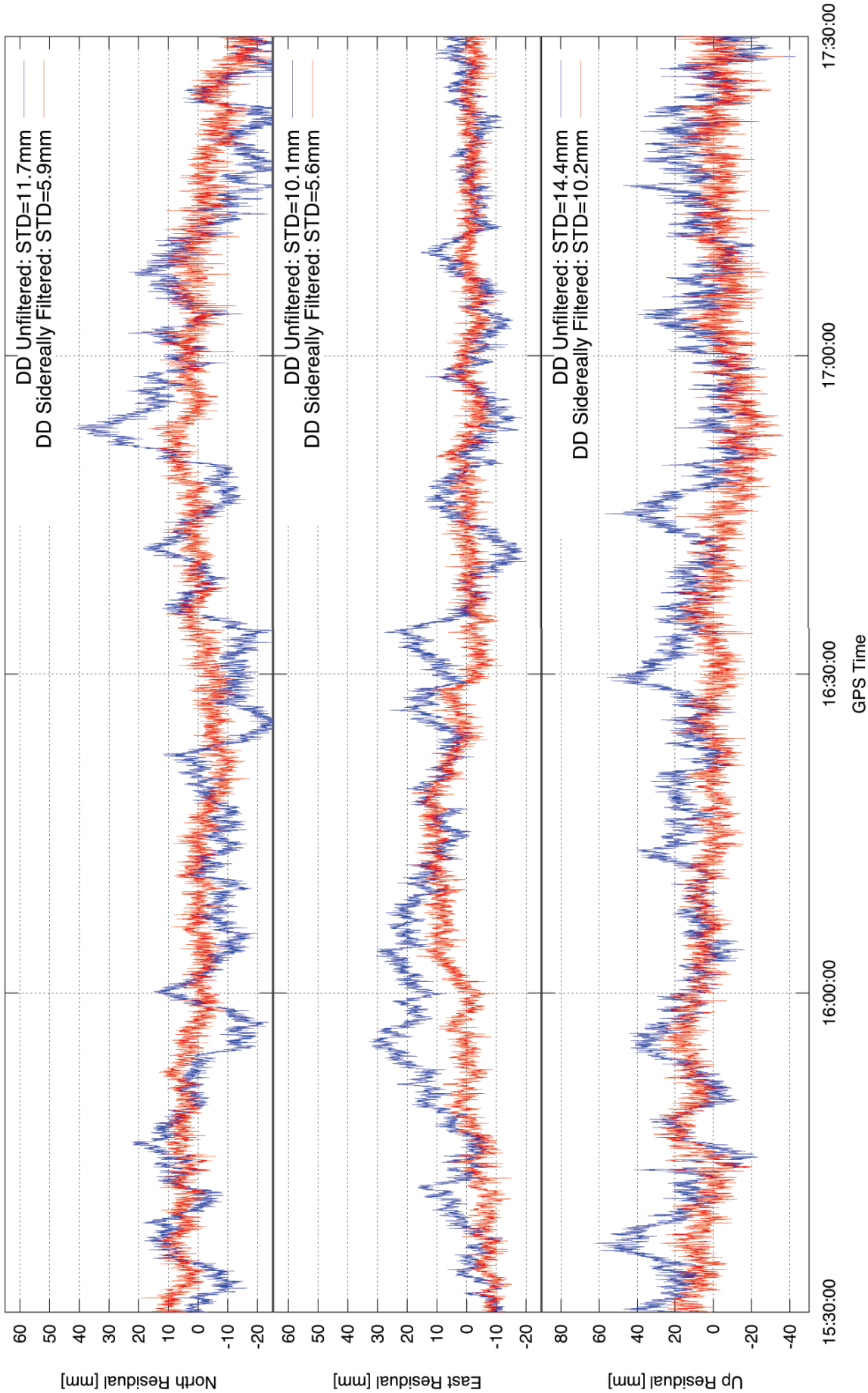

Figure 3.9: Time series for station CRVC, unfiltered (blue) and filtered (red) for DOY 131.

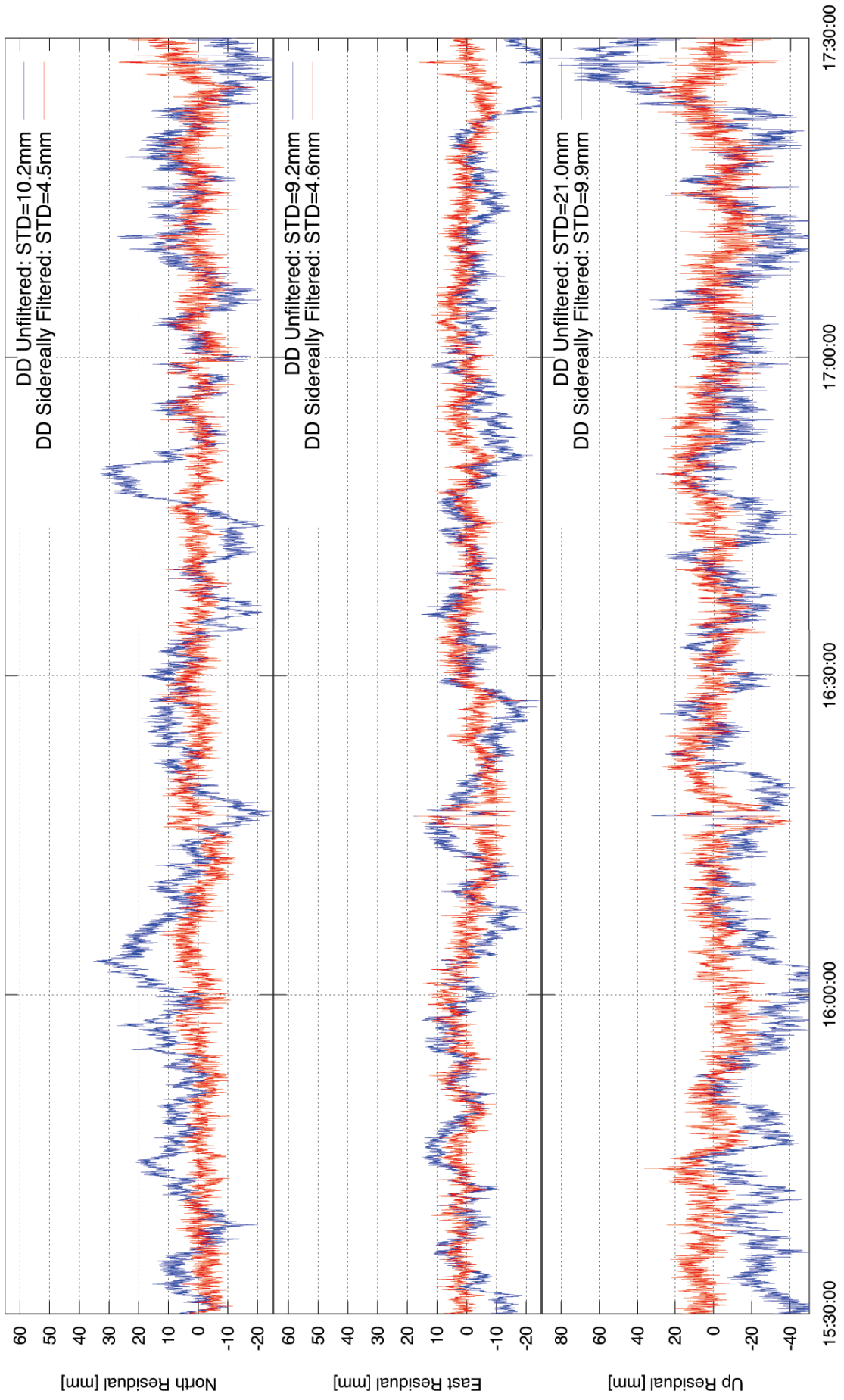

Figure 3.10: Time series for station JUMI, unfiltered (blue) and filtered (red) for DOY 131.

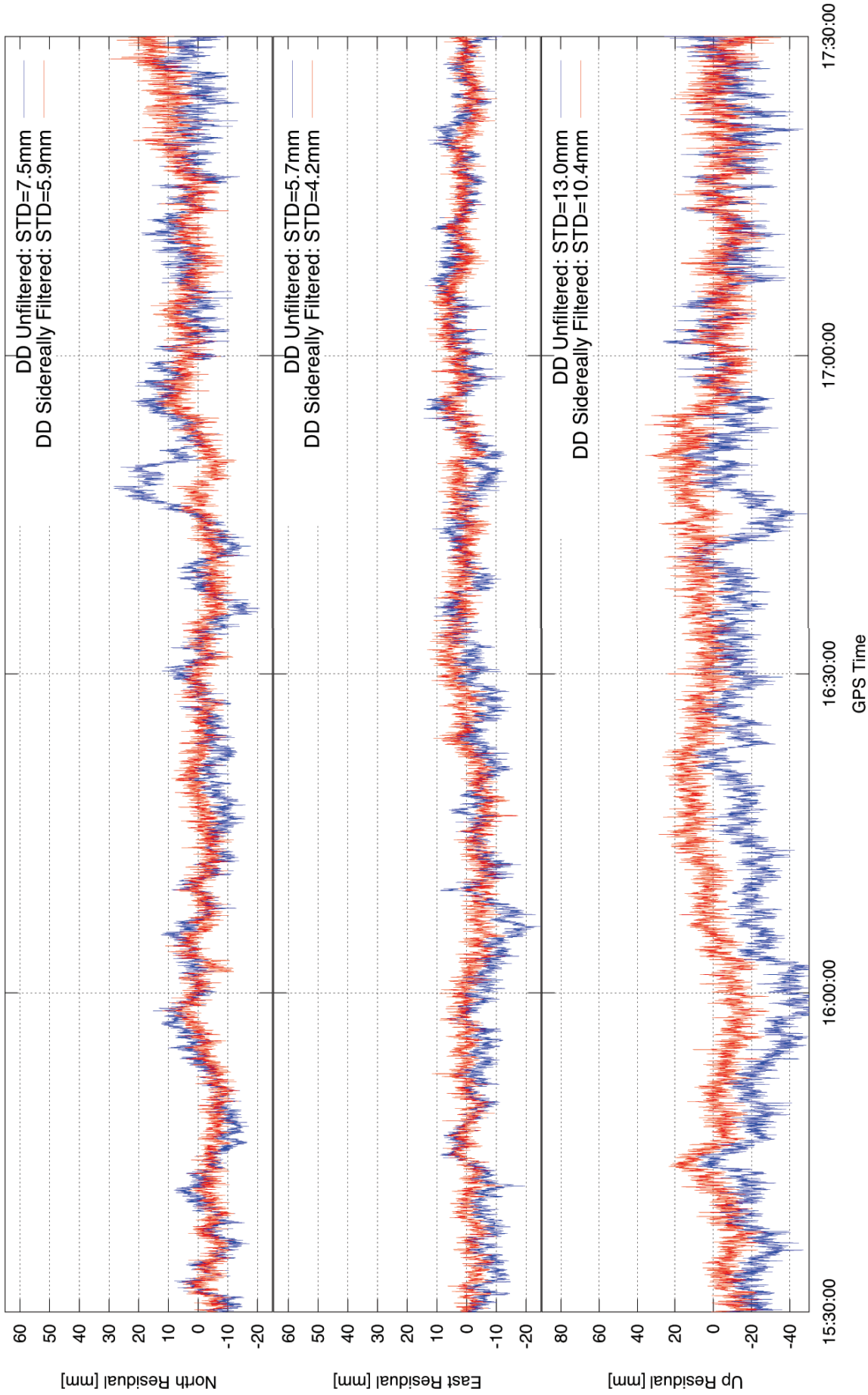

Figure 3.11: Time series for station SALI, unfiltered (blue) and filtered (red) for DOY 131.

Chapter 4

DD and PPP Comparison

Precise Point Positioning (PPP) strategy is an alternative to Double Differencing for GNSS data positioning. PPP is based in the estimation of precise site coordinates and receiver clock corrections independently for each station analyzed [Zumberge et al., 1997]. In this section, sidereally filtered DD data from Chapter 3 is compared with sidereal and regionally filtered[1] (RF) solutions derived from a PPP approach, as stated in [Mendoza et al., 2012].

4.1 Summary

Comparing both strategies, no clear outcome can be stressed. First, a DD approach after MSF leads to a better standard deviation than PPP filtered in the same way for both stations except the E-W component at MURC. On the other hand, when applying both Modified Sidereal and Regional filters to the PPP solutions, results improve visibly. Nevertheless, DD after MSF is still better for LORC station in E-W and vertical components. In any case, the main advantage of a PPP approach is the reduced time needed in order to reach a solution when compared with DD.

LORC	**DD Raw (mm)**	**DD MSF (mm)**	**%**	**PPP Raw (mm)**	**PPP MSF (mm)**	**%**	**PPP MSF+RF (mm)**	**%**
S_N **N-S**	12.0	5.4	**55.0**	7.8	6.4	17.9	3.8	**51.3**
S_N **E-W**	7.5	4.3	**42.7**	5.9	6.5	-10.2	5.6	**5.0**
S_N **Up**	13.6	8.3	**39.0**	14.1	13.6	3.5	12.0	**14.9**
MURC	**DD Raw (mm)**	**DD MSF (mm)**	**%**	**PPP Raw (mm)**	**PPP MSF (mm)**	**%**	**PPP MSF+RF (mm)**	**%**
S_N **N-S**	11.7	6.0	**48.7**	16.7	6.1	63.5	3.9	**76.6**
S_N **E-W**	10.0	5.5	**45.0**	10.9	5.1	53.2	3.5	**67.9**
S_N **Up**	14.3	9.9	**30.8**	44.5	13.7	69.2	9.2	**79.3**

Table 4.1: Empirical standard deviations for LORC and MURC stations, and applied filters. Ratio of improvement between unfiltered and filtered solutions. Time interval considered: from 15:30:00 to 17:30:00 GPST.

[1] A Regional Filter removes spatially correlated influences, this is, eliminates occasional and deterministic common-mode effects influencing all stations in the area in a similar way, but not being related to the periodically repeating satellite constellation. For DD strategy, such effects are intrinsically removed and do not need to be again filtered.

4.2 Time Series

Unfiltered DD and PPP results show better behaviour for PPP in LORC station (Figure 4.2), but for MURC (Figure 4.3), PPP is much more scattered.

After applying only a sidereal filter for every coordinate in both stations, the reduction in standard deviation is bigger for DD than for PPP, excepting E-W for MURC. It can be seen in Figures 4.4 and 4.5, as well as in Table 4.1. However, when comparing MSF applied to the data with MSF+RF applied to the same, the improvement in PPP solutions is evident. Nevertheless, there is no result to point out, if comparing DD + MSF and PPP+MSF+RF. For MURC station, PPP results are clearly better; but for LORC station, DD results standard deviation is better for E-W and height components. This means there is no "best strategy" when related to the results scatter.

In Figure 4.1, a polar plot comparing filtered DD and PPP data is shown. In it, the scatter reduction after filtering PPP results seems bigger for N-S component than for E-W. On the other hand, for DD results, the scatter in both components is similar. Such results are consistent with Table 4.1. Note that both directions are equally scaled.

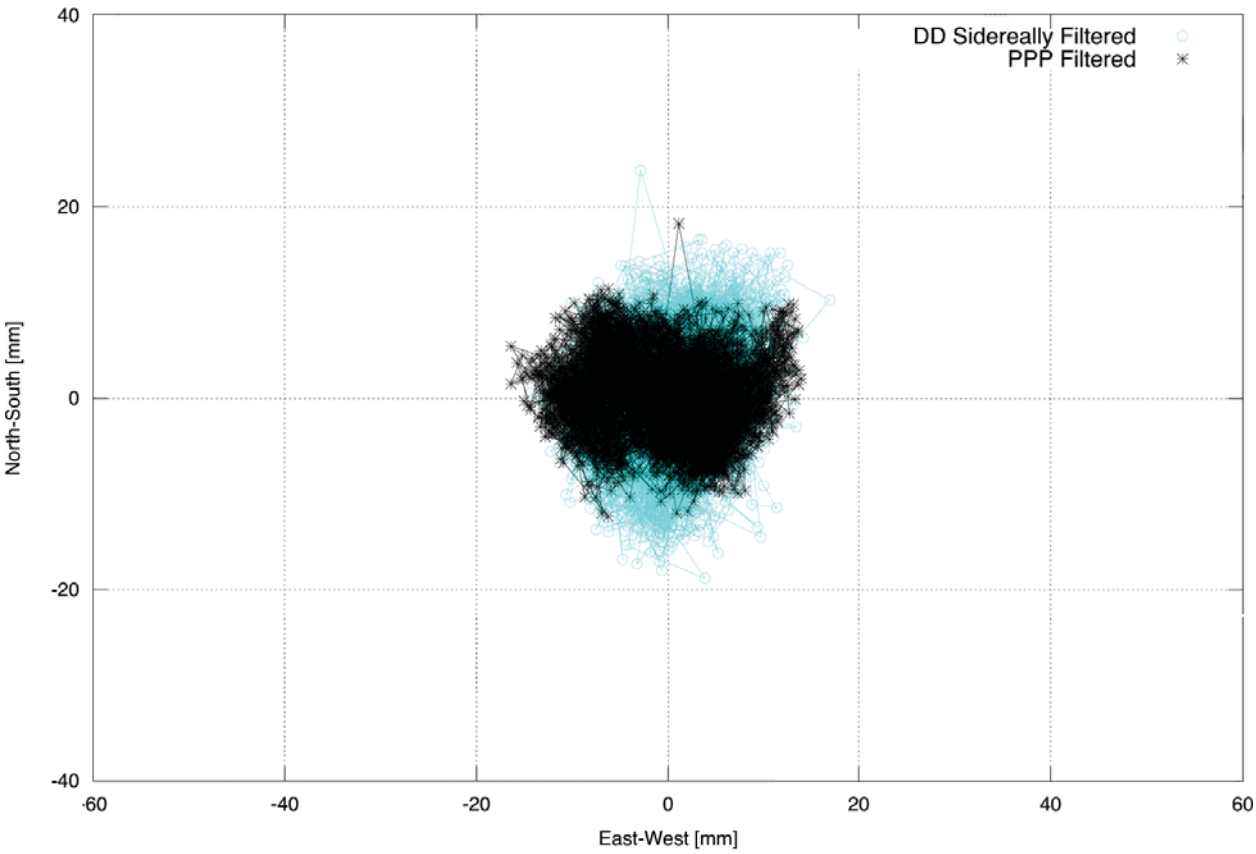

Figure 4.1: Polar plot comparing DD after MSF and PPP after MSF+RF for station LORC.

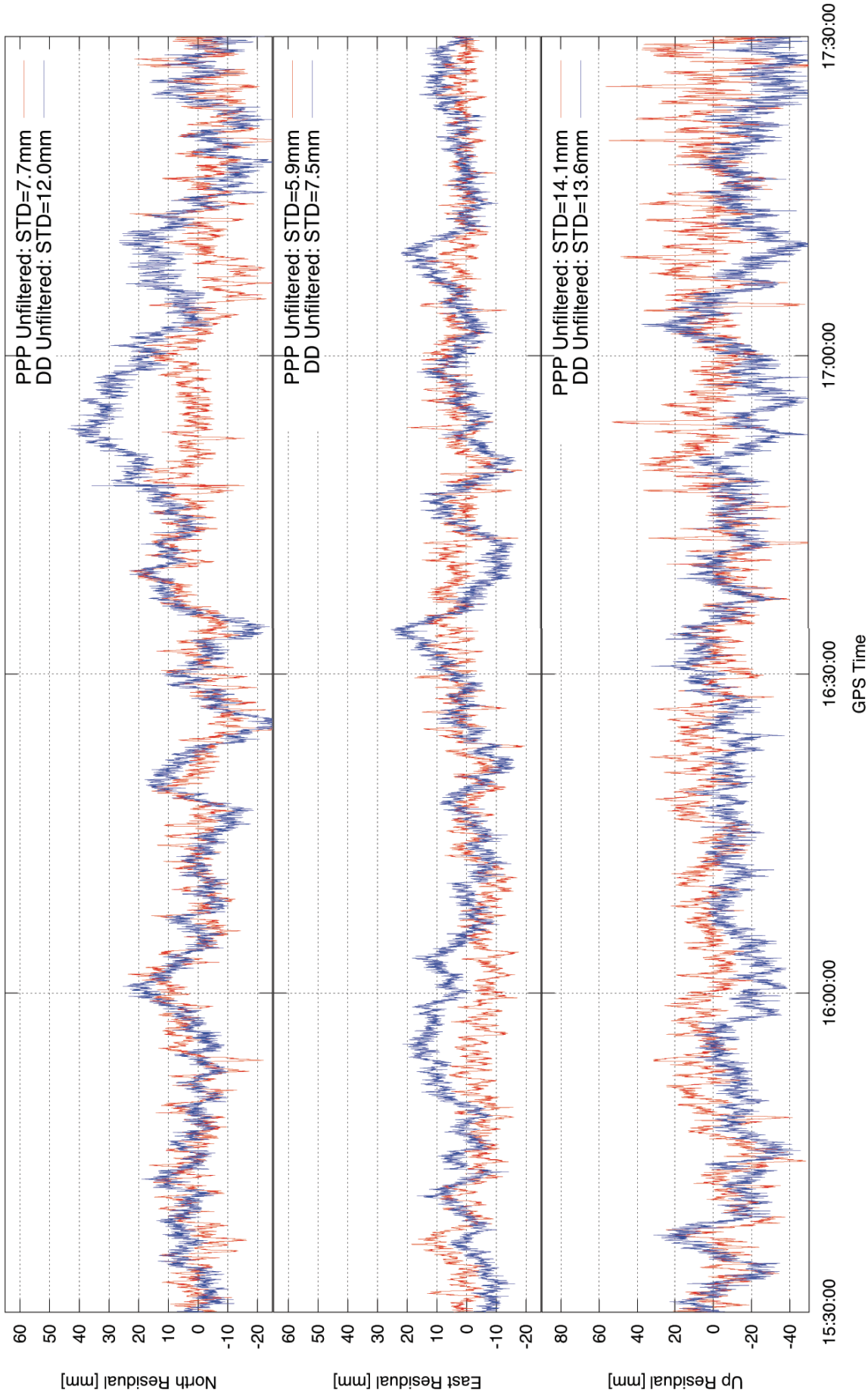

Figure 4.2: Time series for station LORC, unfiltered results from PPP (red) and DD (blue).

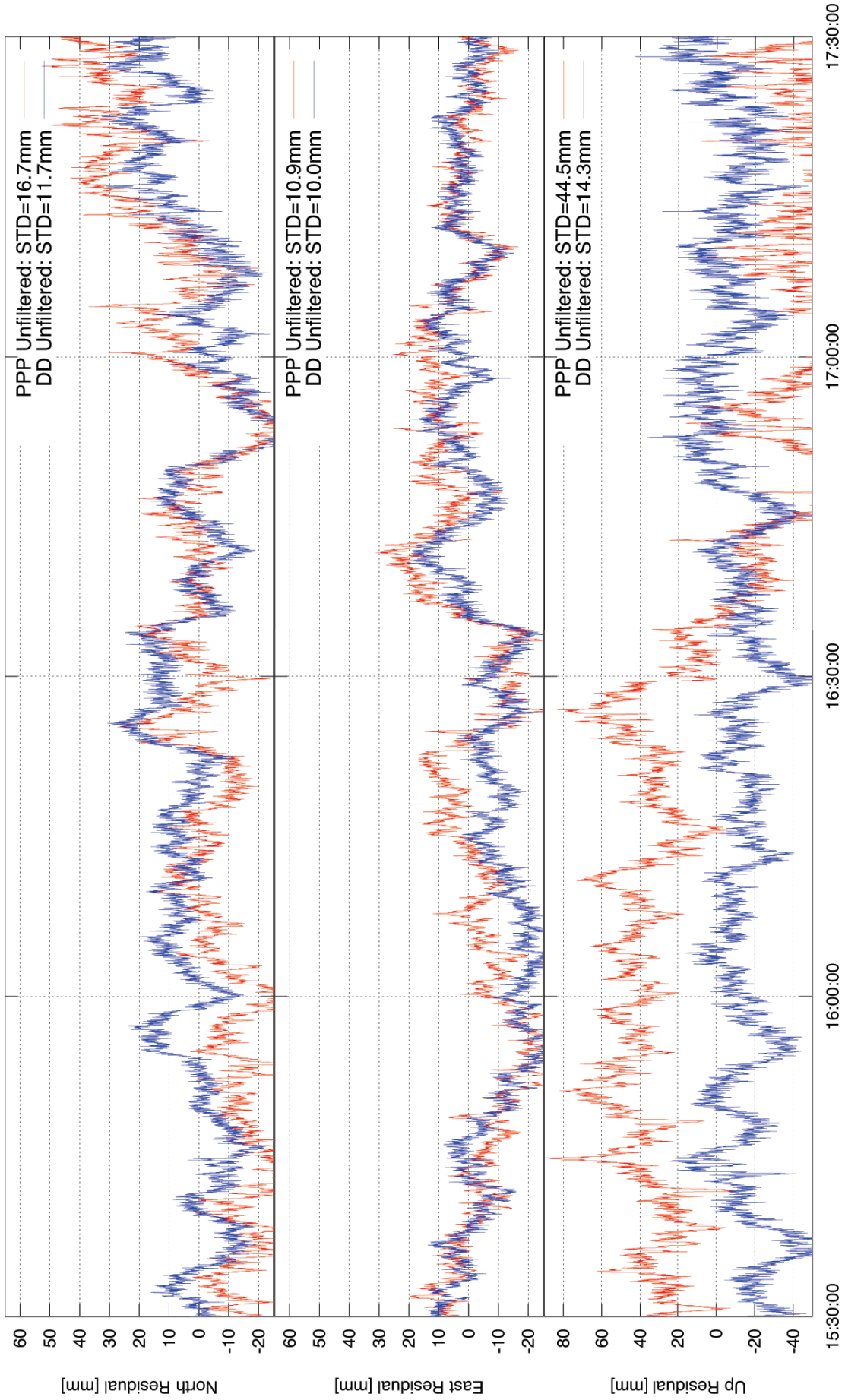

Figure 4.3: Time series for station MURC, unfiltered results from PPP (red) and DD (blue).

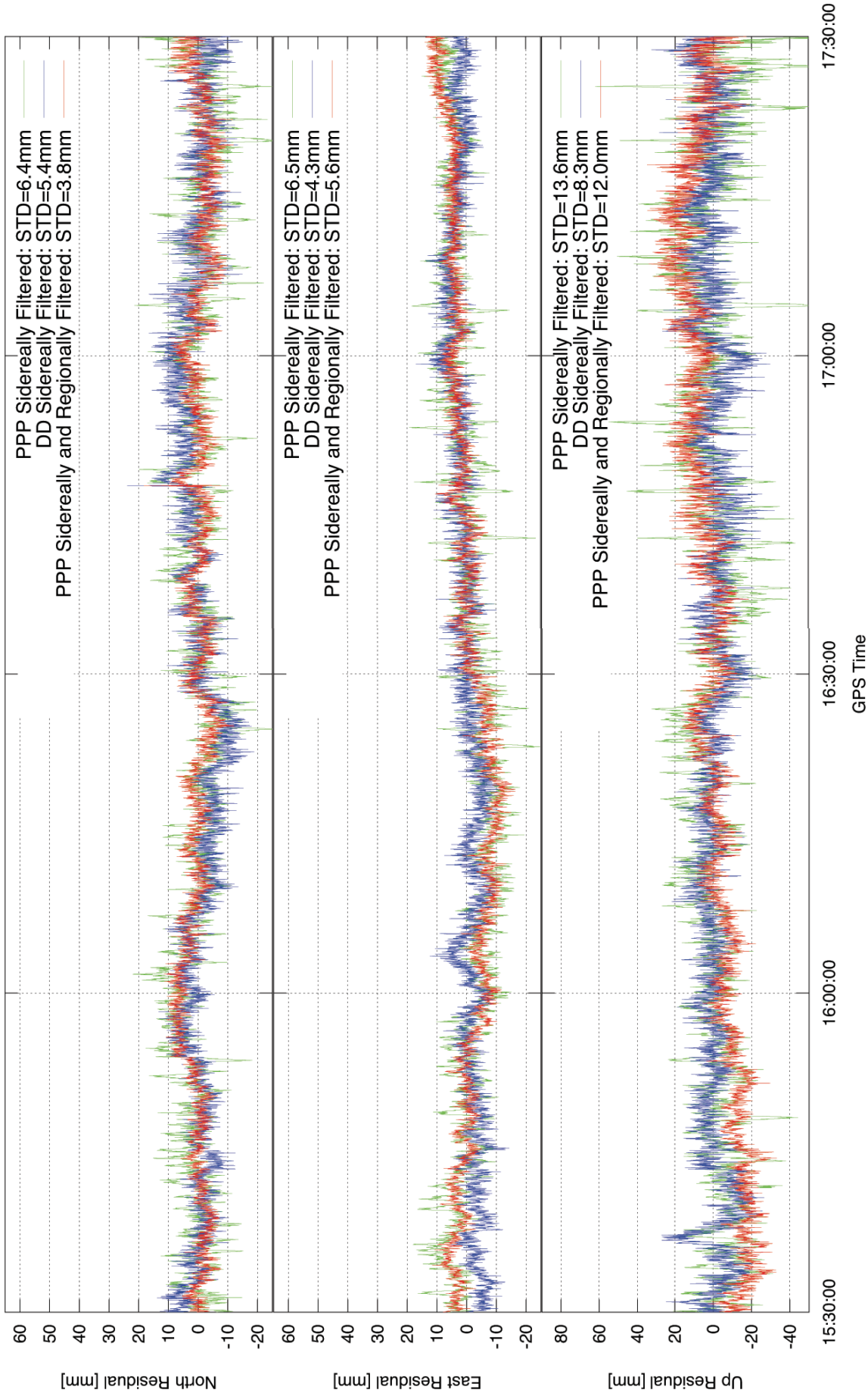

Figure 4.4: Time series for station LORC, filtered results from PPP (green, red) and DD (blue).

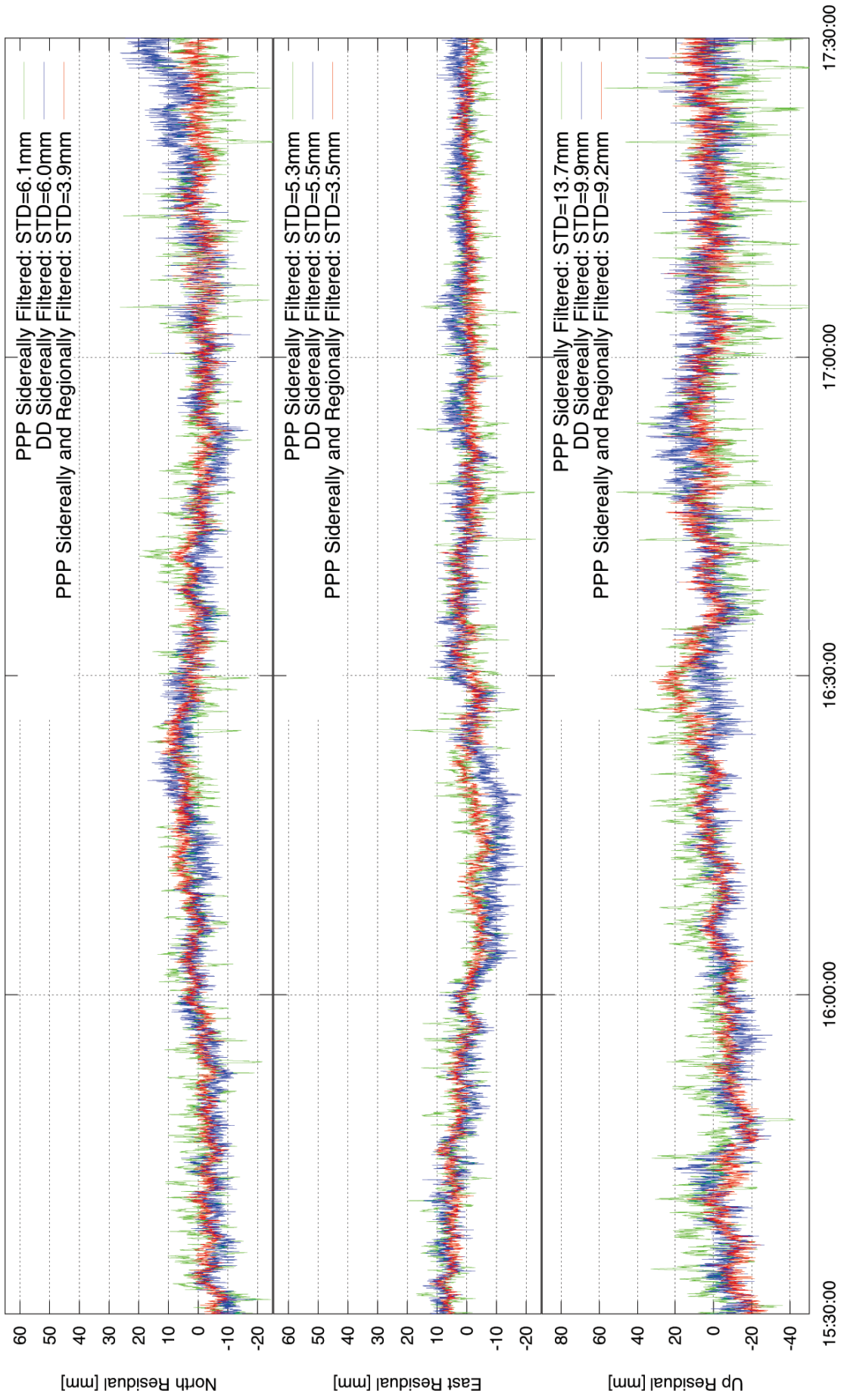

Figure 4.5: Time series for station MURC, filtered results from PPP (green, red) and DD (blue).

Chapter 5

Near-Real Time Analysis

Achieving real time processing is the ultimate goal for every experimental researcher. In order to set up an early-warning system, the best-case scenario is obtaining the station position at the moment it changes its coordinates, essentially real time movement. Nevertheless, data must be processed to get a good estimation of a station's real behaviour. Such a procedure needs some time to be achieved. For the strategy shown in the previous chapters, if processing only one baseline, the ambiguity resolution of 1 hour of data, plus the last 15 minutes kinematic analysis and filtering, takes between 2 and 3 minutes. This must be added to the 15 minutes of delay to get RINEX data from the GPS receivers plus the minute it takes recording and uploading the data files to the Internet. To summarize, an event could be detected between 4 and 19 minutes after it occurred.

5.1 Data Provision

Following the strategy introduced in Section 2.1, RINEX data was downloaded from the Meristemum FTP server, comprising GPSWeek 1635. Ionospheric information was obtained from CODE server. As the goal in this chapter is a simulation of a near-real time procedure, only data available at that time is downloaded: Ultra-Rapid IGS products are fetched from the CDDIS database, instead of final products used in Section 3.1.

5.2 Time Series from 15 Minutes of Output Data

As explained in Section 2.4.2, output from Bernese is obtained every 15 minutes, forming 15 minute data packages. The normal procedure is to take directly the last 15 minutes computed data. A two hours timespan has been plotted for a better understanding.

All the 15 minute data output packages are joined together, and resulting time series are compared with the output obtained from a whole day of processed data. An example of such an obtained result is in Figure 5.1. Clearly, the main problem found is the discontinuity of such time series.

As can be seen in the time series of station LORC in Figure 5.1, some jumps are present in the final time series. This discontinuity in the data rules out the possibility of filtering. A possible reason for such discontinuity is the earthquake occurrence (co- or post-seismic displacement), left outside consideration because earthquake happened at 16:47:42 GPST and the timespan considered here is hours before it. Another reasonable cause for the jumps

is a problem in station LORC itself. Hence, an additional test run is set for station CRTG in baseline JUMI-CRTG for DOY 132 and a different timespan, presented in Figure 5.2.

However, the new time series is also discontinuous. Therefore, the problems are neither station nor earthquake-related (or time-related). Another likely reason is a problem in the troposphere parameters that are included in the last 15 minutes step, previously estimated in the 6 hours run. Such an alternative has also been explored but leads to no improvement in the results. Regrettably this continuity problem is left unsolved in the current report.

5.3 Outlier Screening Method

A typical outlier screening method is studied in this section. This is done by setting a confidence interval of 95%, 3*S_N (empirical sigma) around the mean value.

In order to eliminate outliers in the measurement, a threshold value of 3 times empirical standard deviation is set. This way, epochs with large S_N are found and deleted. Data from stations LORC and MURC are analyzed as an example. Being DOY 131 the day of the earthquake, it is selected to illustrate this procedure.

A slight improvement in the data standard deviation is found after screening, according to the information displayed in Tables 5.1 and 5.2. Nevertheless, as it can be seen in Figures 5.3 and 5.4, this confidence interval does not include all the significant epochs within the time series: some data outside the interval are not actual outliers. In consequence, such a method is not going to be applied for the filtering process.

Station	**Mean**	S_N	**Epochs**
LORC N-S (mm)	-2.56	11.23	97.96%
LORC E-W (mm)	1.69	8.92	97.96%
LORC Up (mm)	-15.58	26.17	97.96%
MURC N-S (mm)	2.50	12.20	98.18%
MURC E-W (mm)	3.66	9.57	98.18%
MURC Up (mm)	-18.54	27.48	98.18%

Table 5.1: Original Data.

Station	**Mean**	S_N	**Epochs**
LORC N-S (mm)	-2.59	10.58	96.71%
LORC E-W (mm)	1.69	8.90	97.92%
LORC Up (mm)	-12.75	21.72	94.27%
MURC N-S (mm)	2.65	11.77	97.63%
MURC E-W (mm)	3.57	9.44	97.90%
MURC Up (mm)	-16.41	24.62	93.74%

Table 5.2: Data within 95% confidence interval.

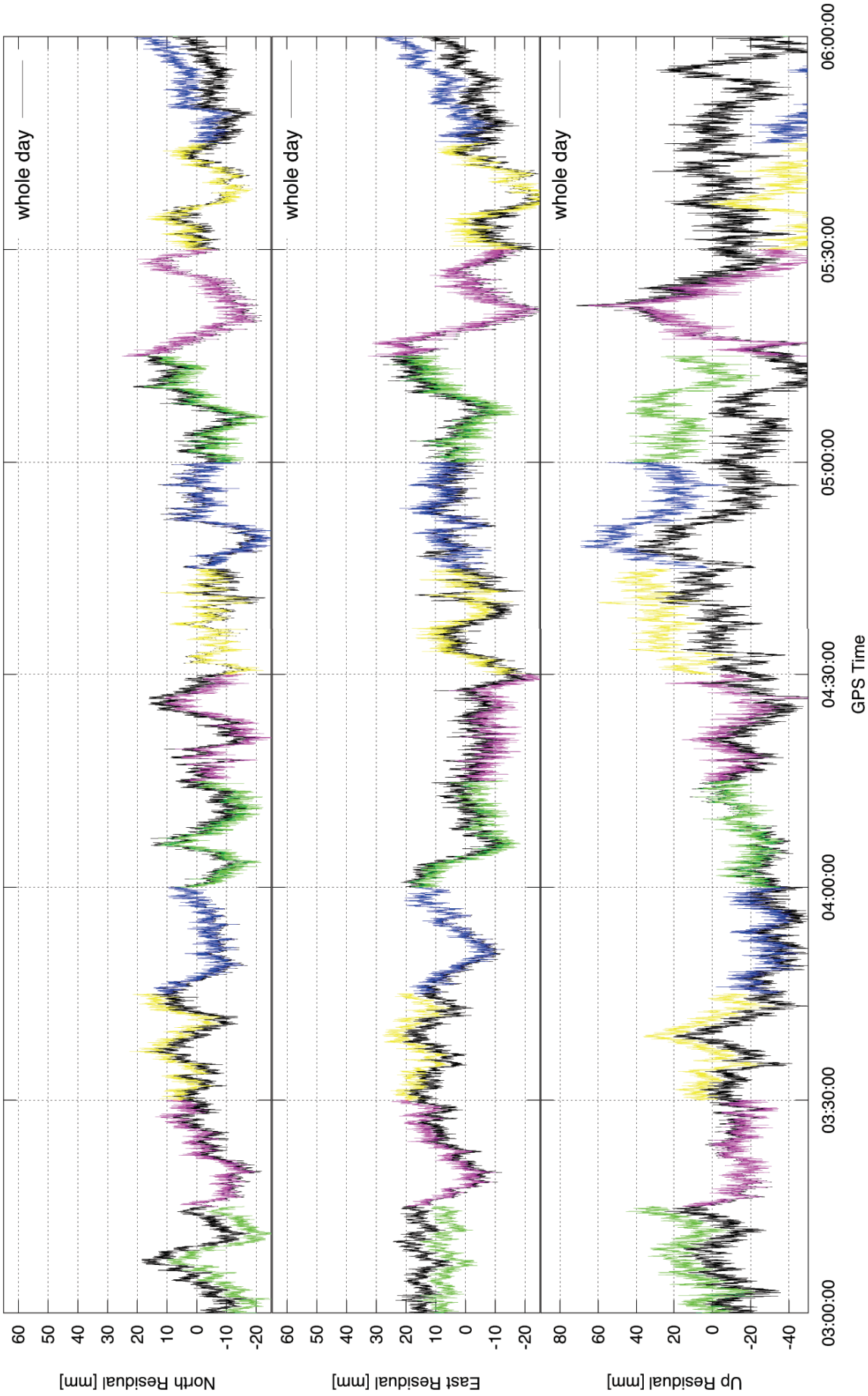

Figure 5.1: Time series for station LORC. 15 minutes joined, versus a whole day of processed data. DOY 131.

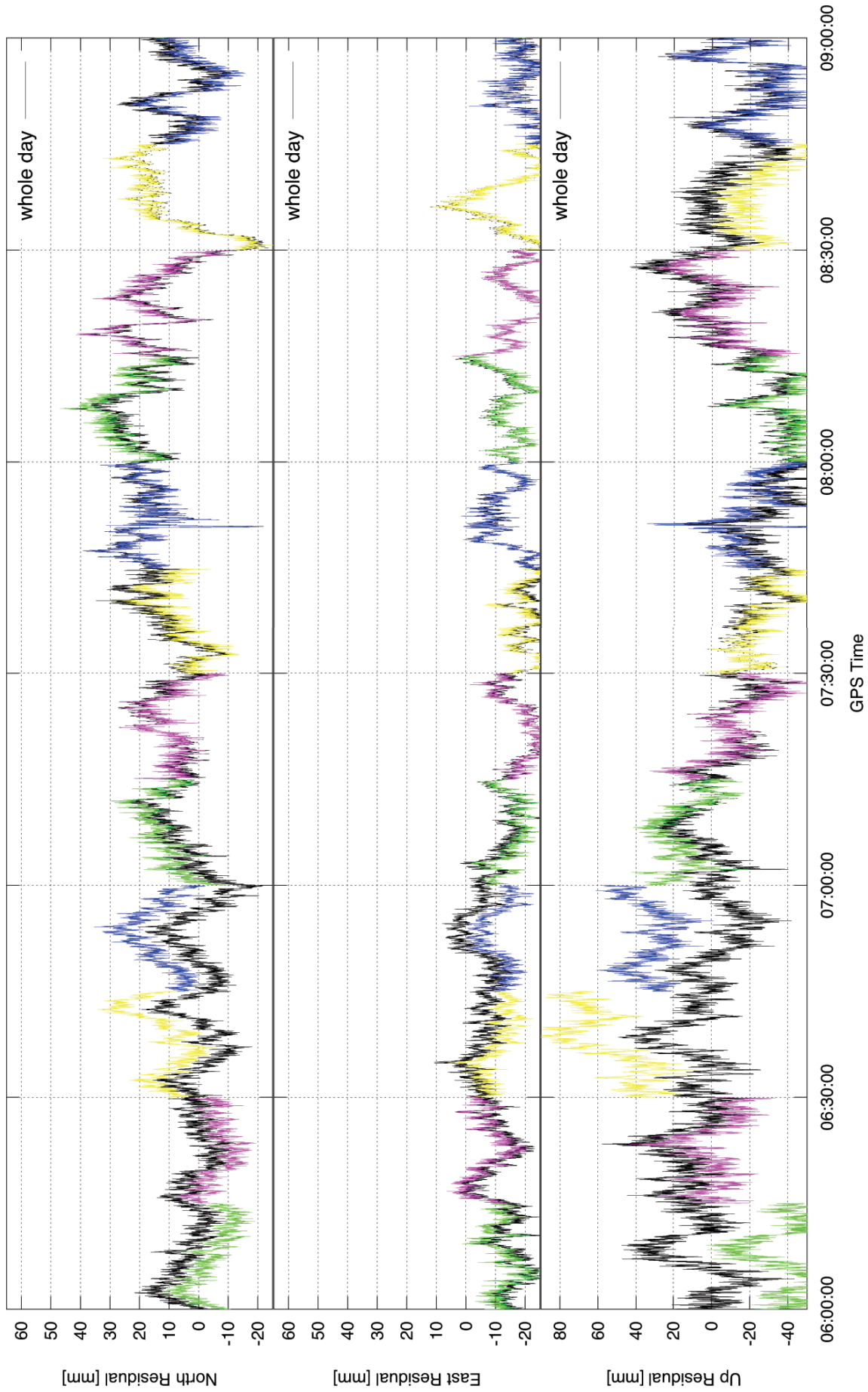

Figure 5.2: 15 minutes time series for station CRTG (in colors). In black, a whole day run. DOY 132.

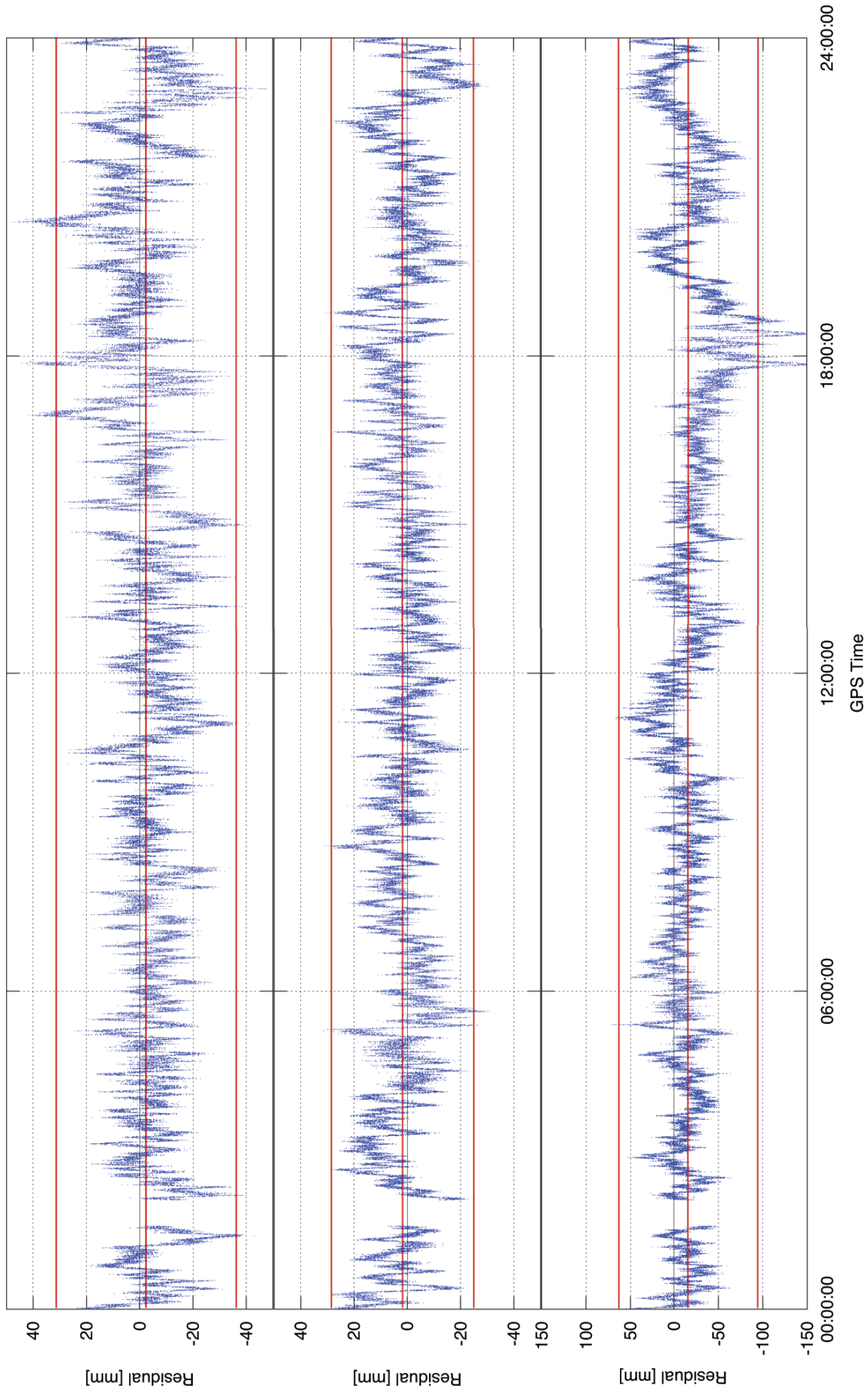

Figure 5.3: Station LORC time series, where red lines correspond to the limits of the 95% confidence interval.

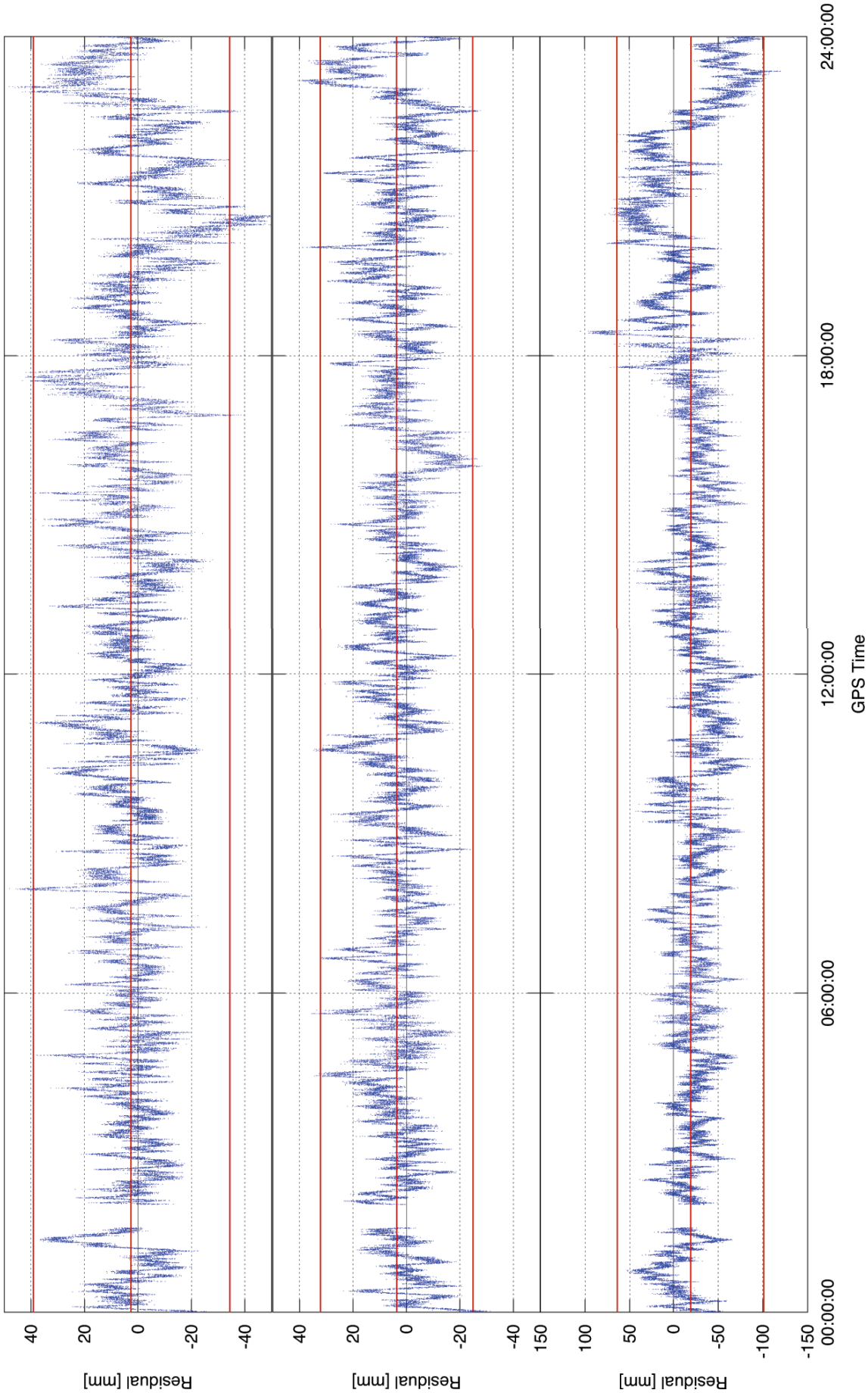

Figure 5.4: Station MURC time series, where red lines correspond to the limits of the 95% confidence interval.

Chapter 6

The Lorca Earthquake

The goal in the previous chapters was to improve the results in order to make possible the seismic waves recognition and amplitude determination, which perturb the time series. Significant periodic oscillations (specially in N-S direction) may be visible shortly after the specified time of the earthquake (16:47:25 UTC) for LORC time series (see Figure 6.1).

Calculations for the earthquake location in the seismic series are achieved using all stations available, including IGN, ROA and UCM among others. Due to the proximity of the equipment, the arrival times have also been used in this calculation. The accelerometer in Lorca, placed very close to the epicenter, enabled the calculation of the hypocenter with a very small error margin. The biggest events in the seismic series are very close and approximately 2 km North of Lorca city, see Table 6.1.

Date	**Time (GMT)**	**Latitude**	**Longitude**	**Depth (Km)**	**Magnitude (M_W)**
11th May 2011	15:05:13	37.7041	-1.6812	2	4.5
11th May 2011	16:47:25	37.6946	-1.6756	3	5.1

Table 6.1: Information from [Cabañas-Rodríguez et al., 2011].

Figure 6.2 shows baseline MURC-LORC processing solutions around the time of the earthquake in near-real time, compared with the apriori solution. Both time series are very similar apart from a slight difference. Amplitude remains unaltered.

6.1 Other Shocks in the Seismic Series

The Lorca earthquake is in fact the biggest event in a series of 149 tremors over three days [López-Comino et al., 2012]. The second biggest shaking had a magnitude of M_W 4.5, and occurred at 15:05:30 GPST on the same day as the main event (information in Table 6.1). The analysis of the station LORC for such event produced a time series shown in Figure 6.3. Peak in N-S component two to three seconds after the estimated arrival time could be considered as an earthquake indicator. Nevertheless, shaking due to an earthquake has a smaller period than what Figure 6.3 shows. Moreover, as there are no more indicators of an anomalous behaviour within, it can be declared that this event is not visible in the correspondent time series.

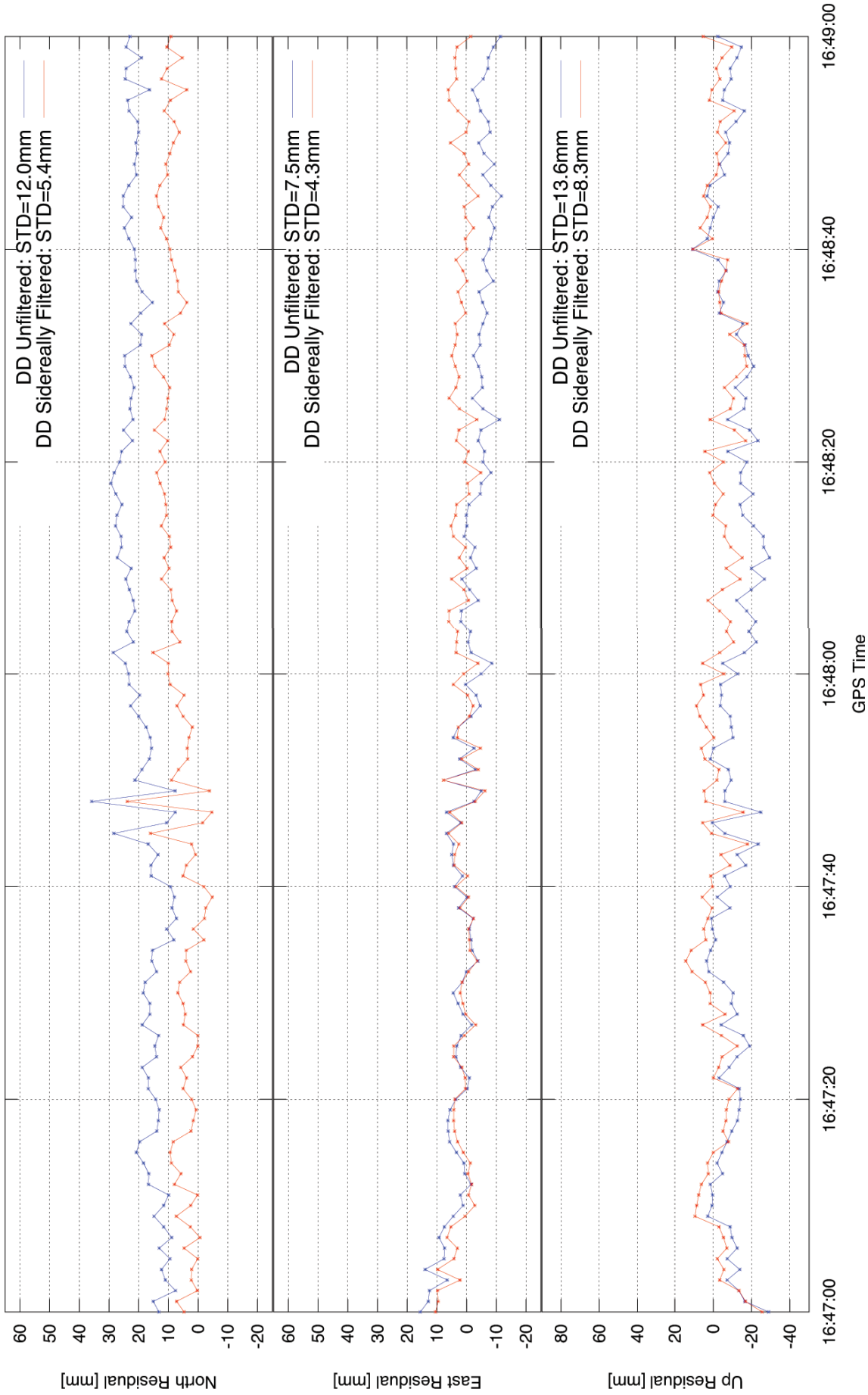

Figure 6.1: LORC time series, DD results before and after MSF.

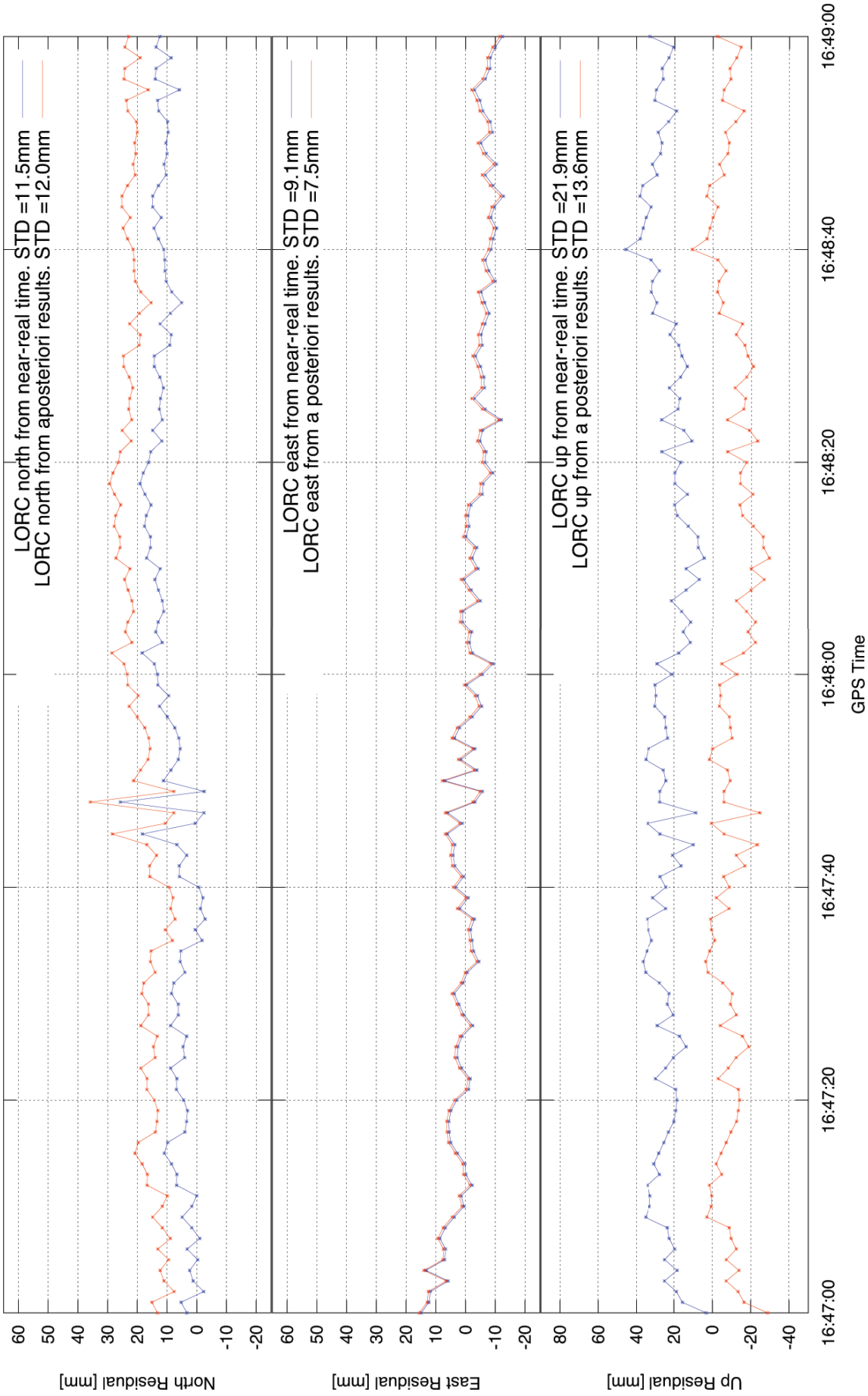

Figure 6.2: LORC time series around the time of the earthquake. Raw results from aposteriori and near-real time data, from baseline MURC-LORC.

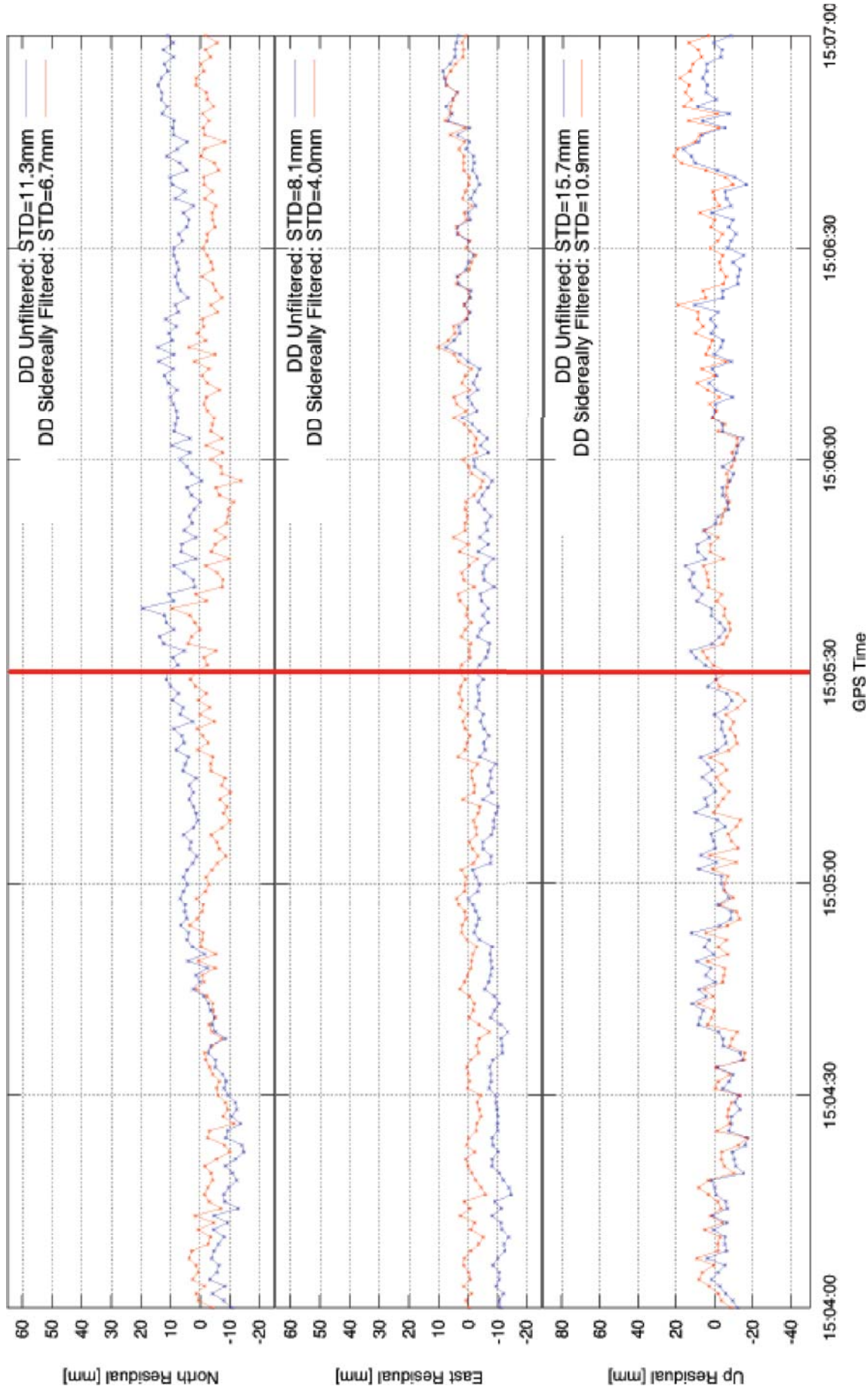

Figure 6.3: LORC time series, DD unfiltered (blue) and filtered (blue), for the estimated time of arrival of the second biggest event in the seismic series at 15:05:30 GPST.

6.2 The Earthquake, as Seen in Seismic Sensors

Accelerometers, as the name suggests, measure acceleration, which must be integrated twice to obtain ground movement. In order to compare with the results from GPS data, the accelerograms from Lorca station, placed 3 km from the epicenter, were recovered.

In Figure 6.4, N-S component is shown. Integration from acceleration to velocity, and from velocity to displacement, smoothens the high-frequency peaks, being the displacement reduced to almost a unique long-period pulse. Its maximum amplitude is 3 cm, agreeing with the signal obtained by GPS in the previous chapters. In [Cabañas-Rodríguez et al., 2011], the maximum amplitude registered during the event is found in N30^{o}W direction.

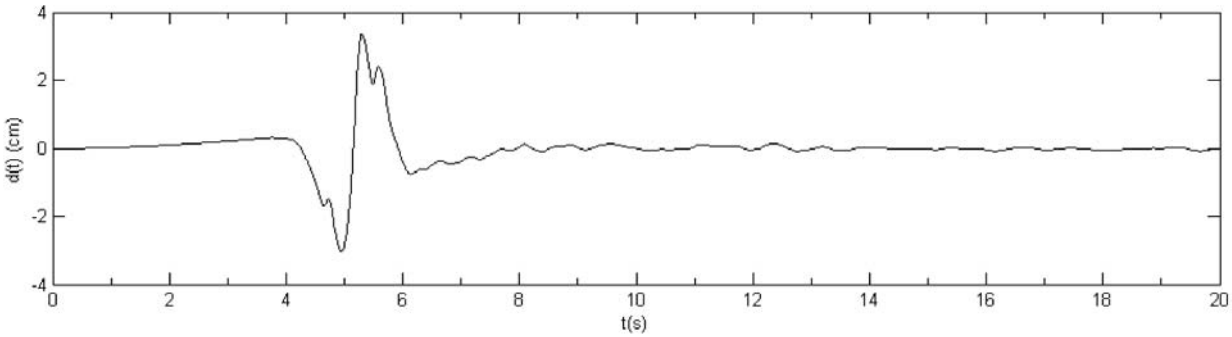

Figure 6.4: N-S displacement over time of the accelerometer near Lorca (station Lorca), after double integration from the signal. Filter 0.1-50 Hz. Taken from [Cabañas-Rodríguez et al., 2011].

6.3 Comparison of Different Baselines

The behaviour of the measurements registered during an event depends on the position of the considered station with respect to the fault. In addition, slight changes between the stations in the network can influence the goodness of the results. In this section, solutions obtained after analyzing all possible baselines containing LORC station are studied. Time series around the instant of the earthquake are compared depending on the baseline considered and statistics are derived from data recorded within one hour before and after the event. LORC station position is set as kinematic, while the rest of the stations are held static.

Figure 6.5 shows the graphical representation of the solutions using all the aforementioned baselines for a minute before and after the event. One of the most interesting results in this report is that station LORC overall behaviour is definitely different depending on the baseline used to obtain its position. Nevertheless, the movement of LORC station during the earthquake (starting at 16:47:42 GPST) is almost identical for each baseline: amplitudes are very similar and the duration of the shaking is also much the same. As a consequence, for this particular event, the baseline used for the shaking detection and amplitude estimation is irrelevant.

It is also interesting to consider the orientation of the baselines with respect to the fault (see green lines in Figure 3.1). LORC-MURC baseline is almost parallel to the fault, while LORC-CRTG and LORC-CRVC are almost perpendicular to it. LORC station derived from LORC-SALI baseline shows the best performance in terms of standard deviation, according to the information displayed in Table 6.2, as well as the biggest ratio of ambiguities resolved (Table 6.3). Nevertheless, the theory states that the most significant displacements are found in baselines parallel to a fault. For this reason, solutions for station LORC are always derived from LORC-MURC baseline, being in this case the closest to the fault direction.

		DD Raw	DD MSF	%
LORC-MURC	S_N N-S (mm)	12.0	5.4	**55.0**
	S_N E-W (mm)	7.5	4.3	**42.7**
	S_N Up (mm)	13.5	8.3	**39.0**
LORC-CRVC	S_N N-S (mm)	8.9	6.1	**31.5**
	S_N E-W (mm)	9.4	8.4	**10.6**
	S_N Up (mm)	12.5	8.7	**30.4**
LORC-JUMI	S_N N-S (mm)	9.0	6.1	**32.2**
	S_N E-W (mm)	9.3	8.4	**9.7**
	S_N Up (mm)	12.5	8.7	**30.4**
LORC-CRTG	S_N N-S (mm)	7.4	5.3	**28.4**
	S_N E-W (mm)	6.5	5.1	**21.5**
	S_N Up (mm)	13.0	11.4	**12.3**
LORC-SALI	S_N N-S (mm)	5.8	4.7	**19.0**
	S_N E-W (mm)	5.3	4.7	**11.3**
	S_N Up (mm)	12.0	10.3	**16.7**

Table 6.2: Empirical standard deviations for the different baselines with LORC in one end. DD solutions before and after applying the MSF. Ratio of improvement between unfiltered and filtered solutions. Time interval considered: from 15:30:00 to 17:30:00 GPST.

Baseline	**Strategy**	**% Resolved**
CRTG-LORC	WL-NL	96.3
CRVC-LORC	WL-NL	94.5
JUMI-LORC	WL-NL	96.4
MURC-LORC	WL-NL	90.7
SALI-LORC	WL-NL	98.1

Table 6.3: Ratio of solved ambiguities, strategy used and baseline considered.

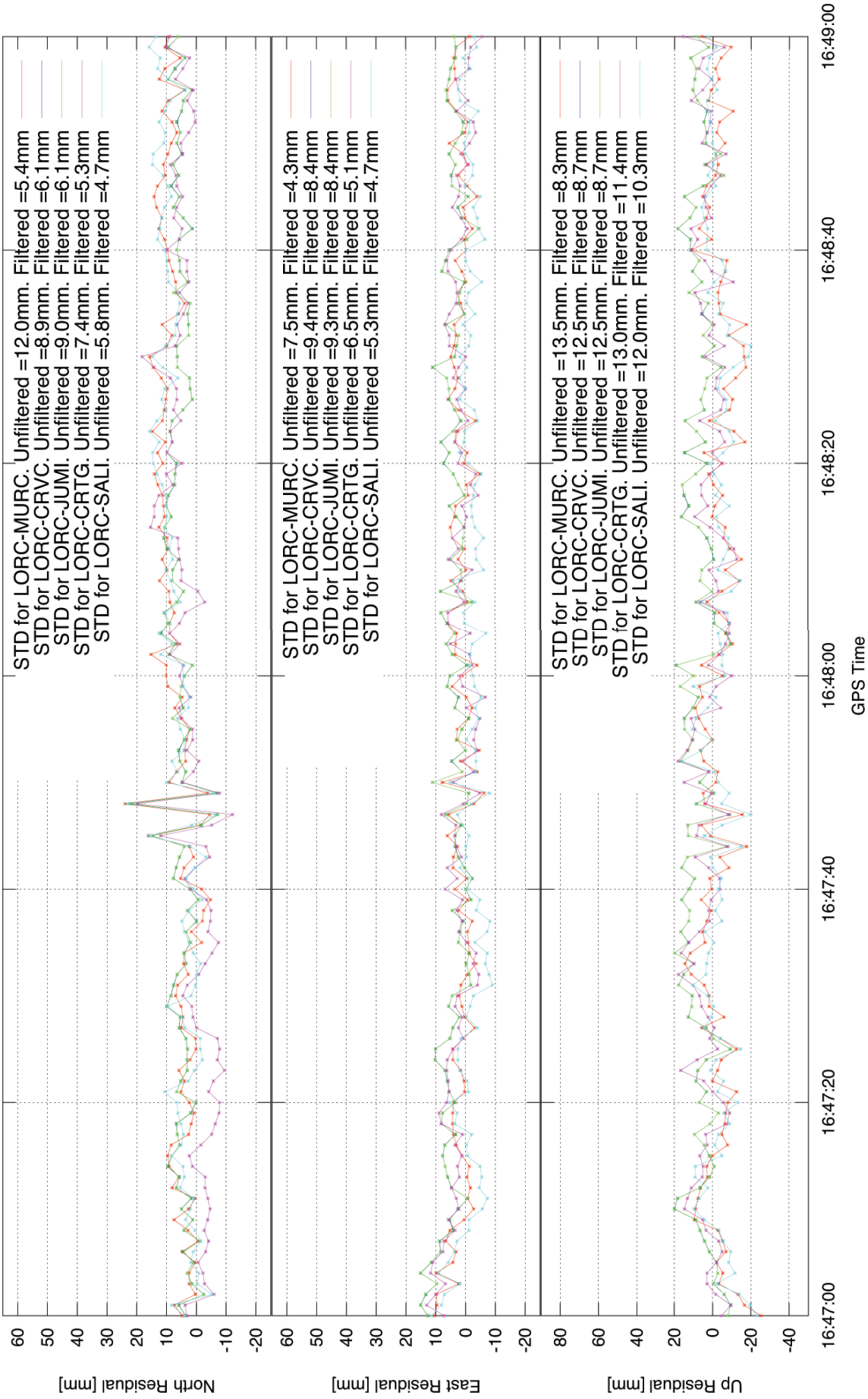

Figure 6.5: Time series around the time of the earthquake for station LORC (kinematic) and the rest of stations (static) in the network.

6.4 The Earthquake in Other Stations

Since earthquake waves propagate radially from the hypocenter and they travel in different ways through the layers of the ground, depending on the type of material they cross, an approximation of the propagation velocity may be calculated. The given earthquake origin time is 16:47:40 UTC and the movement in the station LORC begins at 16:47:42 UTC, placed 5.1522 km away from the epicenter. As the hypocenter was shallow, the distance between it and each station is taken as the linear distance in the surface. Then, the arrival times to the different stations for the earthquake waves are as in Table 6.4.

Station	**Epicentral Distance (km)**	**Est. arrival time (GPST)**
LORC	5	16:47:42
CRVC	49	16:47:59
MURC	58	16:48:02
CRTG	62	16:48:04
SALI	80	16:48:11
JUMI	91	16:48:15

Table 6.4: Distance to the epicenter and estimated arrival times.

In Figures 6.7 and 6.8, MURC and CRTG time series from DD after MSF applied are shown, timespan between 16:47:00 and 16:49:00 GPST. The expected arrival time is marked as a vertical red line for each station. Despite the fact that the aforementioned stations are the nearest to the epicenter (after LORC), it turns out that they do not show any distinct movement in the time series in any coordinate. No displacement is detectable in the rest of stations as well, see Figures 6.9, 6.10 and 6.11.

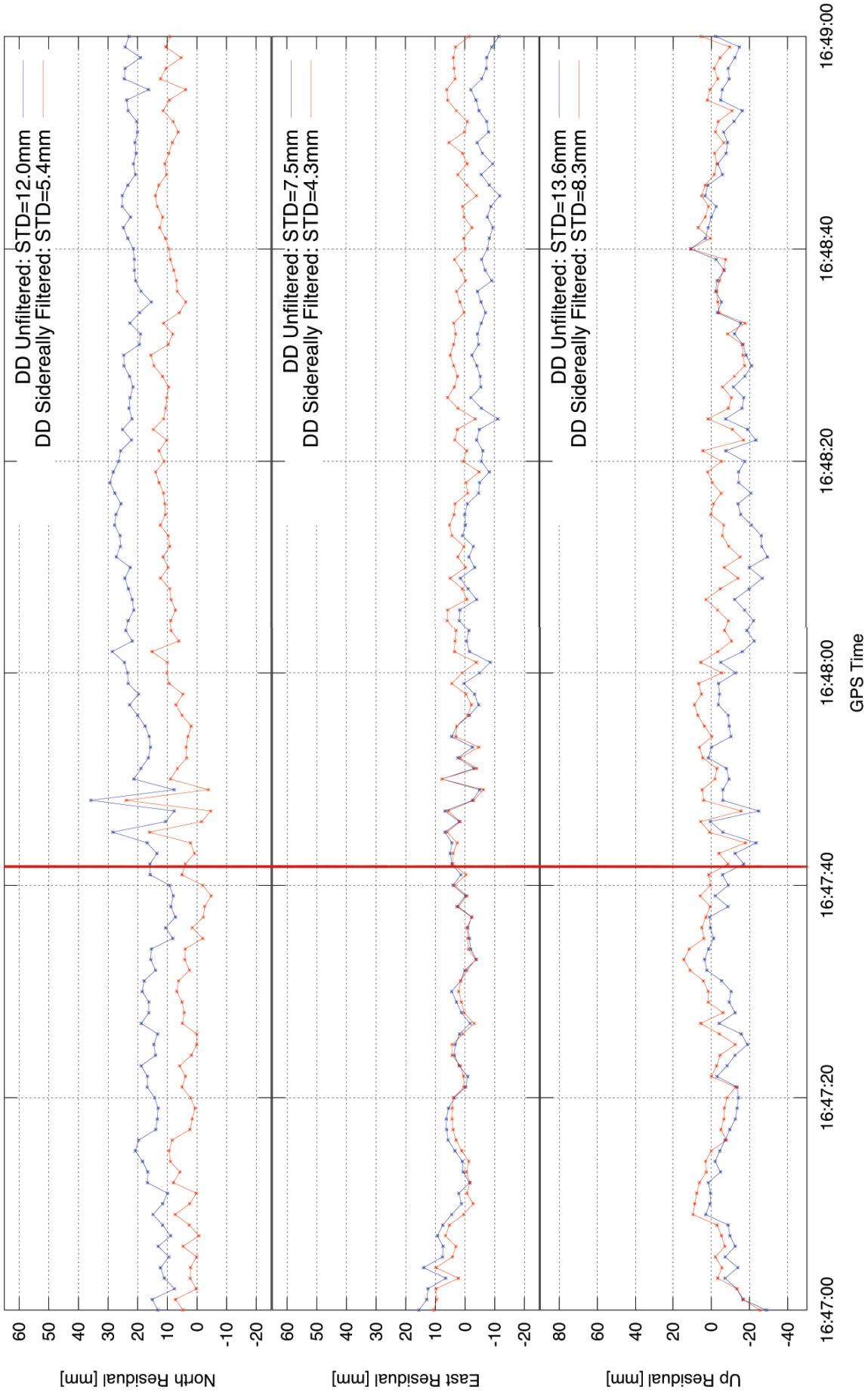

Figure 6.6: LORC time series, DD unfiltered (blue) and filtered (blue).

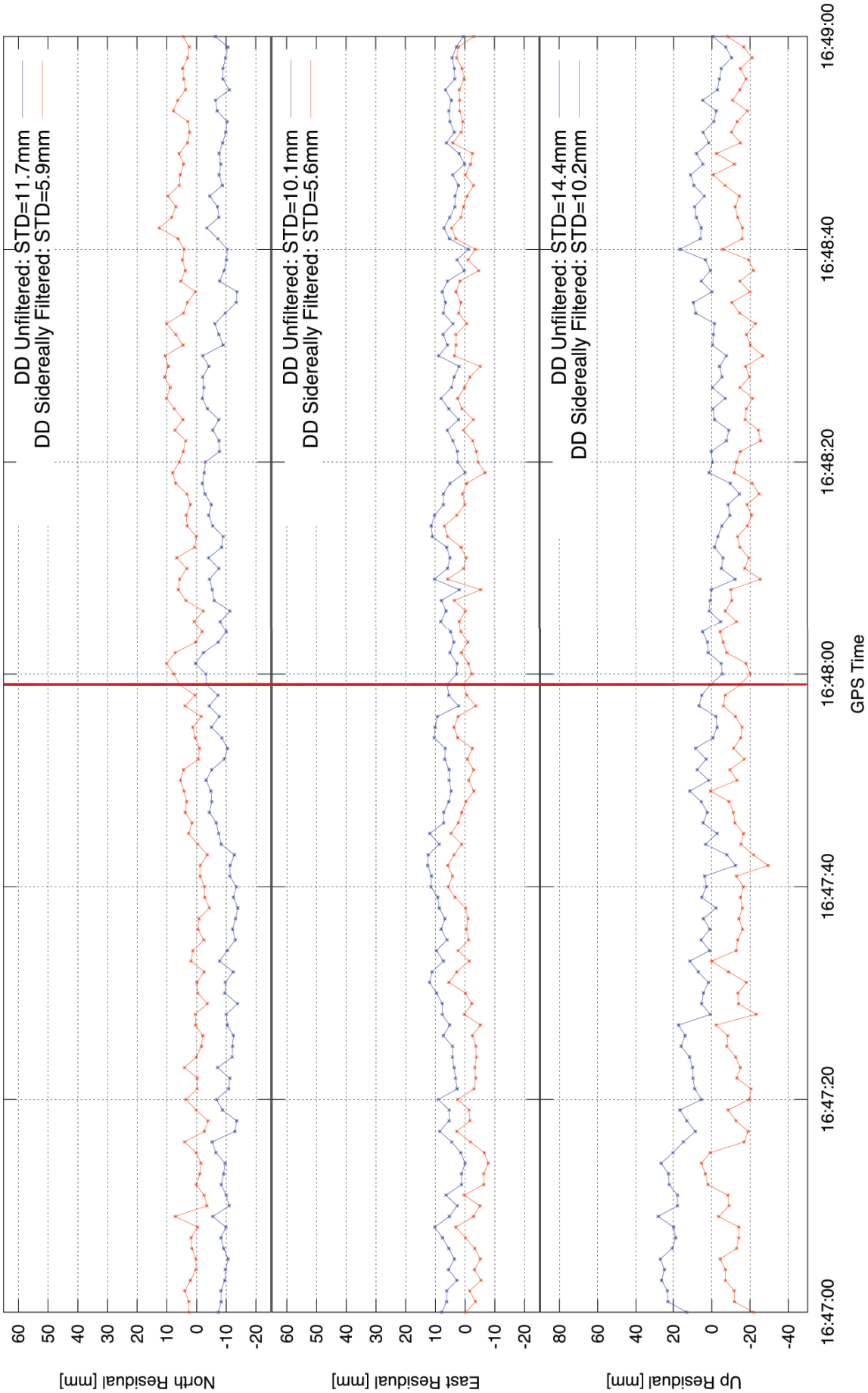

Figure 6.7: CRVC time series, DD unfiltered (blue) and filtered (blue).

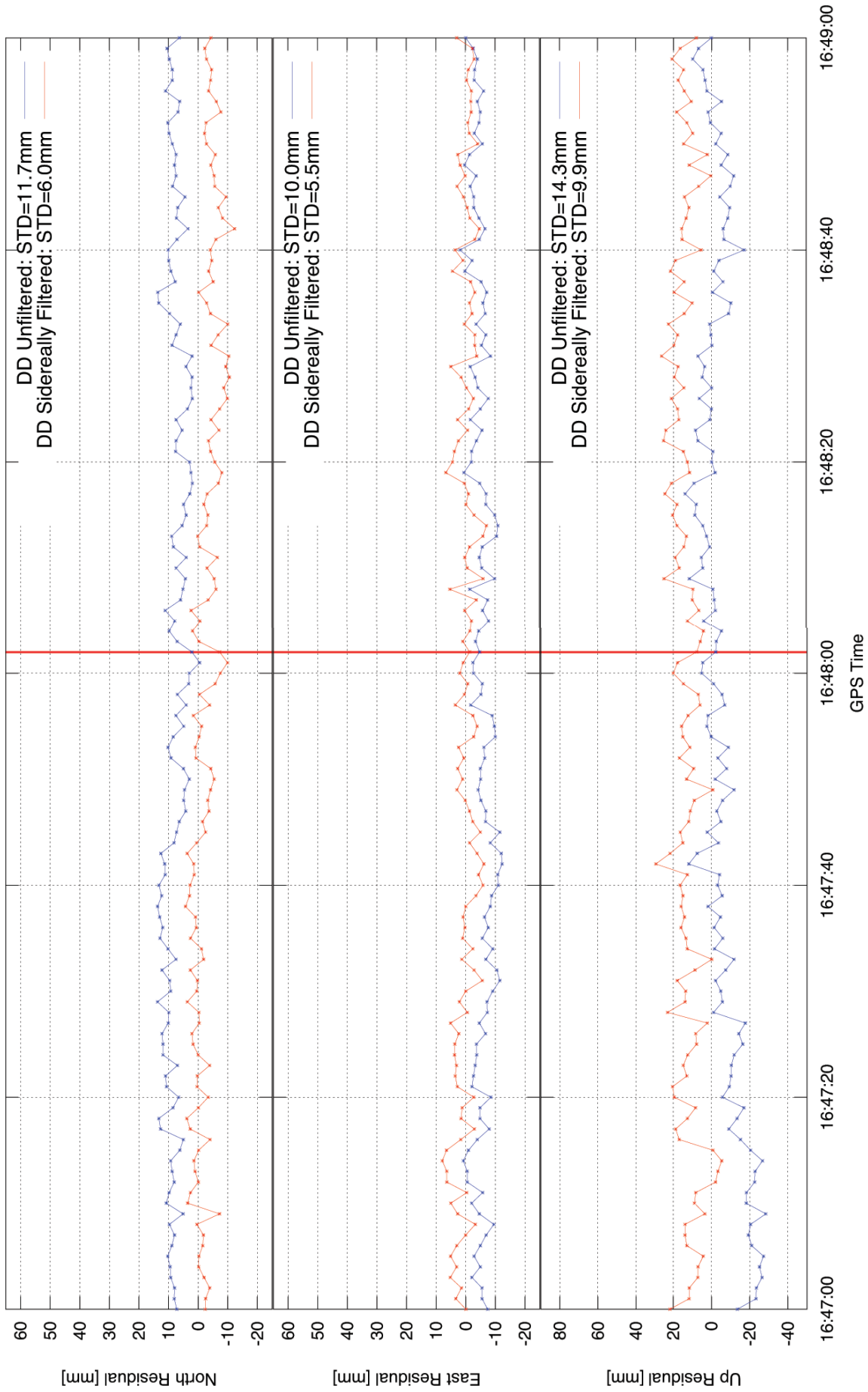

Figure 6.8: MURC time series, DD unfiltered (blue) and filtered (blue).

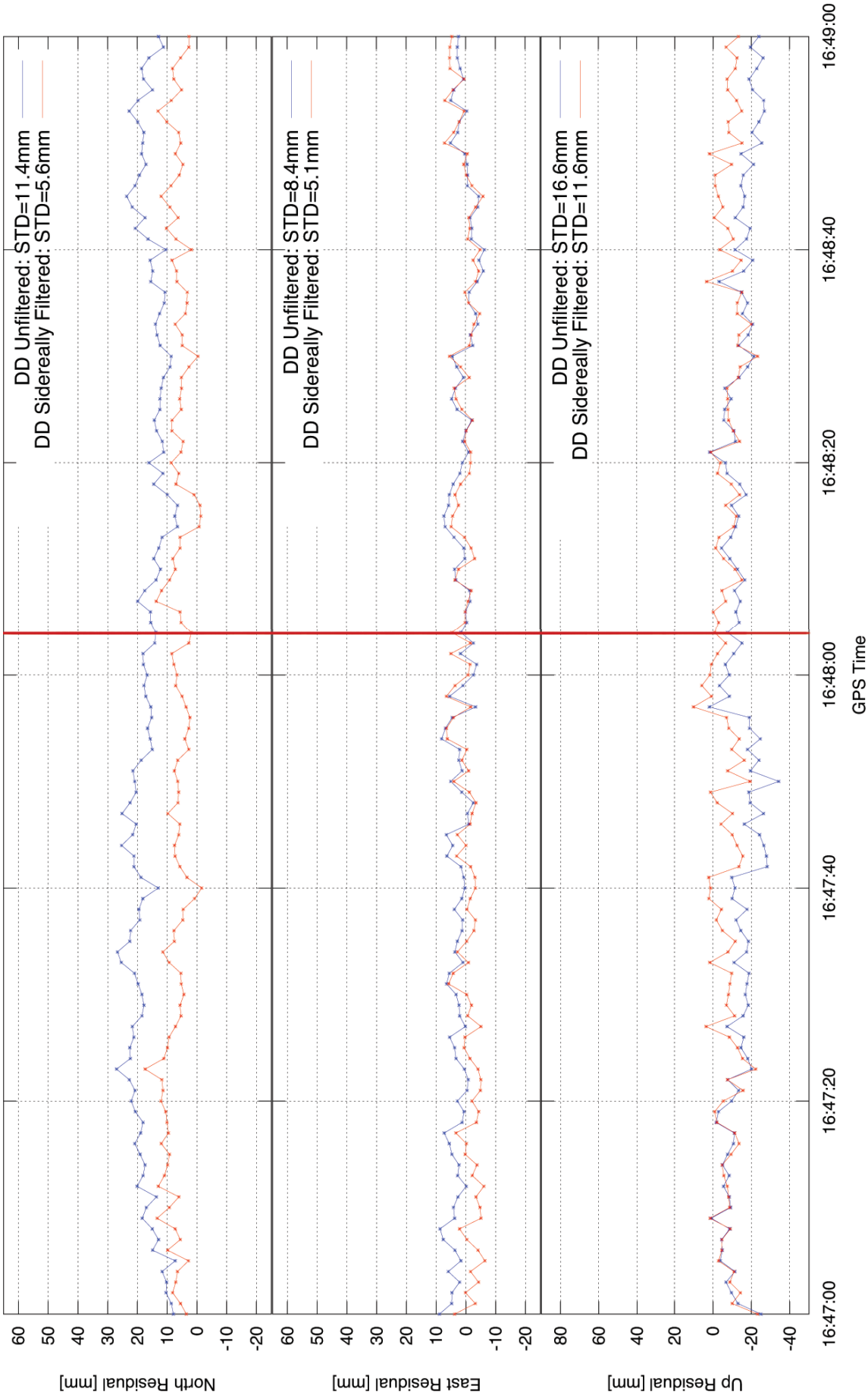

Figure 6.9: CRTG time series, DD unfiltered (blue) and filtered (blue).

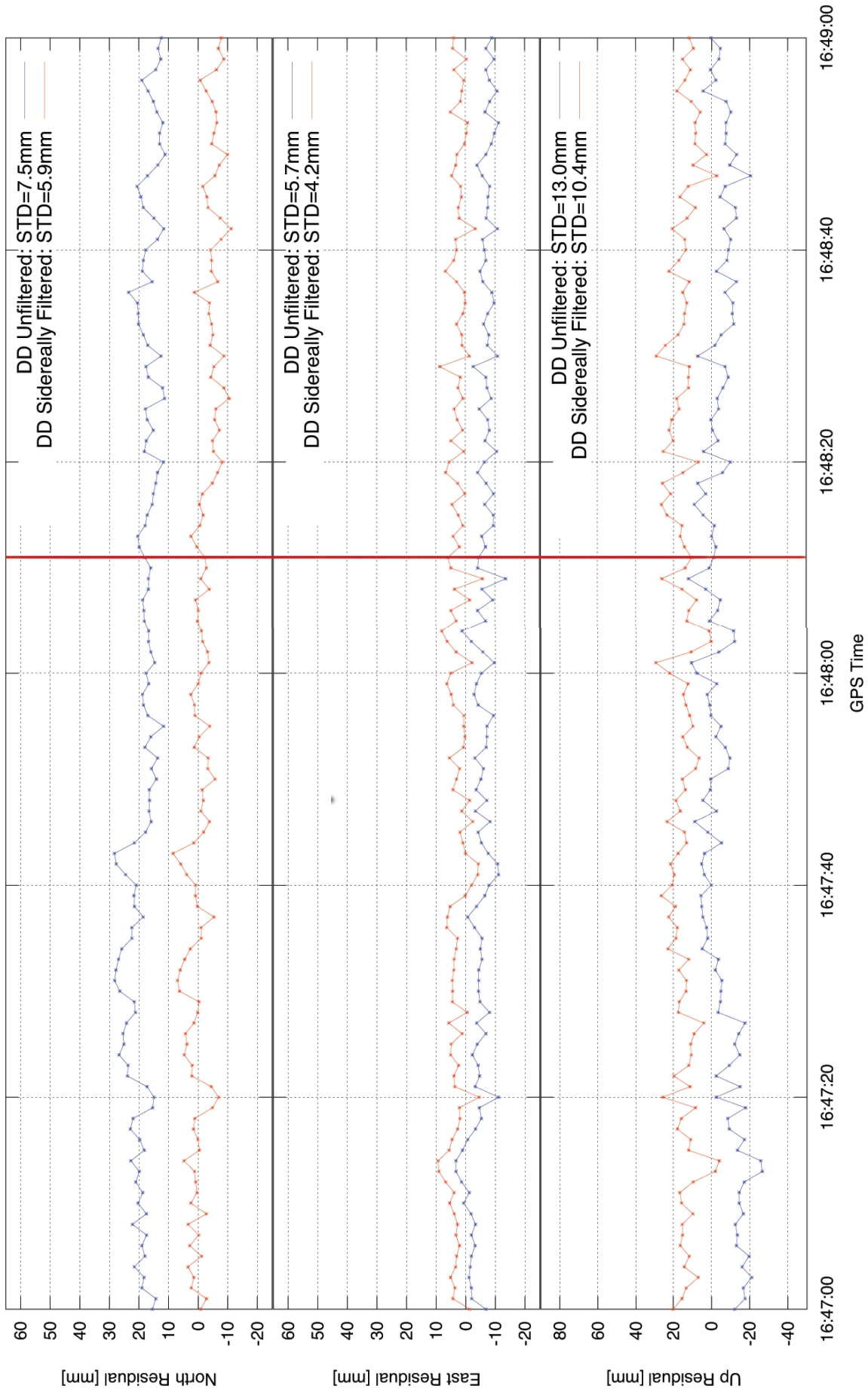

Figure 6.10: SALI time series, DD unfiltered (blue) and filtered (blue).

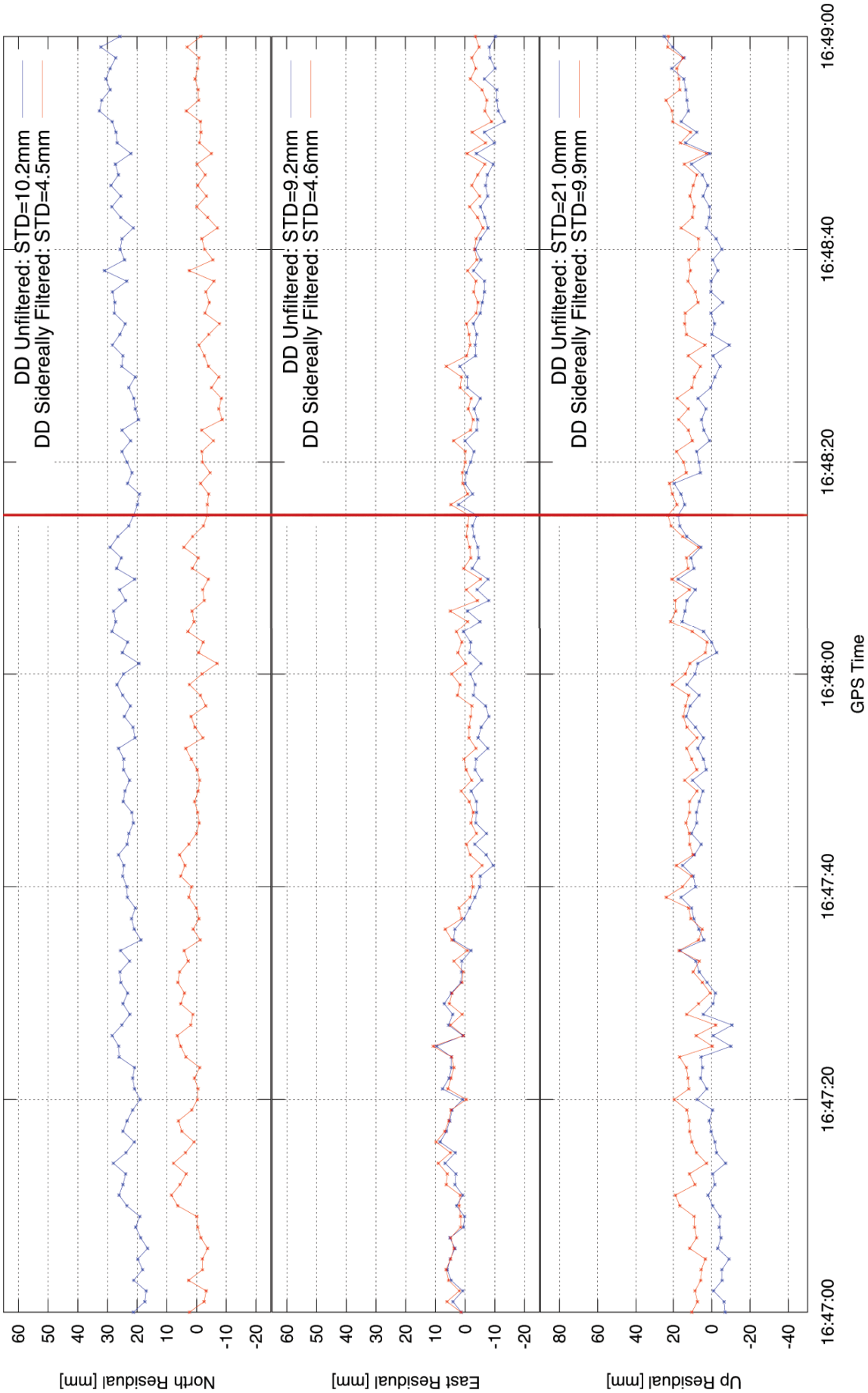

Figure 6.11: JUMI time series, DD unfiltered (blue) and filtered (blue).

Chapter 7

Conclusions

Real time analysis has been developed in the last few years. Its strength is based on the availability of streaming data and good-quality satellite orbit information. A GPS capable of measuring, storing and delivering 1 Hz data can be used to directly measure dynamic ground displacements generated by medium to large earthquakes, as well as landslides, volcanoes and tsunamis.

Proper kinematic coordinate analysis is highly time-consuming. If processing more than 6 stations in kinematic mode, the current run overlaps with the following 15 minutes interval. Despite BPE enables automatic analysis for the kinematic coordinates, overlapping should not happen.

Kinematic coordinates accuracy is a very important point when generating time series. When few observations are available, it is found that the standard deviation is of tens of centimeters. Therefore, timespans with less than 85% of data available are not reliable.

Using the Modified Sidereal Filter, time series satellite configuration error constant part is reduced. The studied timespan is of a week for the overall and two hours around the earthquake for the concrete. For the time of the earthquake, a solution per second within two minutes around the event is shown, and its scatter reduction is clear.

In this report, the past Lorca earthquake (May 11th, 2011) is studied using GPS data with DD and PPP techniques. Results obtained between days 128 and 134 of year 2011 reveal ground movement between 1 and 3 cm. Time series display peak-to-peak displacements up to a maximum of 2-3 cm in N-S and 2 cm in E-W as well as in height. The GPS receiver position in Lorca correlates well with the distance to the epicenter and with the area of maximum shaking. Seismological data matches up as well, after double integration of the accelerogram. Therefore, both peak-to-peak movement and arrival time can be explained directly from the direction of the rupture and the composition of the ground. It agrees with other results, for example the recent paper from [López-Comino et al., 2012].

Another interesting result obtained in this report comes to the study of different baselines with LORC station in an edge. In Figure 6.5, the time series for each possible baseline containing LORC station are plotted. Clearly, LORC behaviour is different in each time series, but not for the record of the earthquake, where its movement (and also peak-to-peak amplitude) is almost identical. This is, as remarked in Section 6.3, the baseline used in the shaking detection and amplitude estimation is not relevant, at least for this event.

Outlook

Over the last years, an increasing number of permanent GPS networks have been deployed in many regions of the world. The large amounts of data that can be daily measured by GPS receivers demand a very high level of automated analysis. Such measurement surveys take over several weeks or even months. Bernese BPE can execute all possible tasks in batch mode or in parallel, and in automatic mode. An early-warning system could benefit from this, alerting authorities about incoming earthquakes. With the support of seismical results, scientists and risk managers can analyze real time data, defining warning levels and communicating with local residents in case of an extreme hazard.

For a future application with GALILEO satellites, it must be stressed that the GALILEO constellation has its own orbital period of 14 hours and orbit repeat time of approximately 7 days. Moreover, GLONASS satellites have an orbit period of 11 hours and 15 minutes, and its orbit repeat time is approximately 8 days. This has to be considered when setting up the MSF. Data from GLONASS satellites were not used for this investigation.

Further research must be carried out in order to guarantee the continuity of the time series in near-real time processing. This is a key point in order to apply a proper filter to the data obtained in near-real time. Moreover, if implementing NTRIP flow data, the processing could be made available in a few minutes, instead in the $\sim$20 minutes that this approach can provide.

Acknowledgements

Let me take this opportunity to show my most sincere gratitude to several institutions and people without whom this project could have never came to light:

First of all, the Alvargonzález foundation for making this research possible.

Then, the San Fernando Naval Observatory (ROA) as institution, especially to Jorge Gárate Pasquín and José Martín Dávila, for their kind support and help.

Also, the Institute of Geodesy of Darmstadt Technical University, in particular to Professor Matthias Becker for tutoring me throughout the research process.

I should not forget to mention the public FTP services of the Consejería de Agricultura y Agua of the Murcia Region [http://www.carm.es/cagric] and the International GNSS Service [Dow et al., 2009] for their high-quality data and products.

Last but not least, I would like to show my appreciation to Alexander Kehm and Axel Koppert for sharing the results of their analysis using a different processing method.

Bibliography

[Agnew and Larson, 2007] Agnew, D. C. and Larson, K. (2007). Finding the repeat times of the GPS constellation. GPS Solutions *11*, 71–76.

[Beutler et al., 2008] Beutler, G., Bock, H., Dach, R., Fridez, P., Gäde, A., Hugentobler, U., Jäggi, A., Meindl, M., Mervart, L., Prange, L., Schaer, S., Springer, T., Urschl, C. and Walser, P. (2008). Bernese GPS Software ver. 5.0 Manual [Online]. Astronomical Institute, University of Bern.

[Cabañas-Rodríguez et al., 2011] Cabañas-Rodríguez, L., Carreño-Herrero, E., Izquierdo-Álvarez, A., Martínez-Solares, J. M., del Villar, R. C., Martínez-Díaz, J., Benito-Oterino, B., Gaspar-Escribano, J., Rivas-Medina, A., García-Mayordomo, J., Perez-López, R., Rodríguez-Pascua, M. A. and Murphy-Corella, P. (2011). Informe del sismo de Lorca del 11 de mayo de 2011. Technical report . Instituto Geográfico Nacional de España.

[Dow et al., 2009] Dow, J., Neilan, R. E. and Rizos, C. (2009). The International GNSS Service in a changing landscape of Global Navigation Satellite Systems. Journal of Geodesy *83*, 191–198.

[Gonzalez et al., 2012] Gonzalez, P. J., Tiampo, K. F., Palano, M., Cannavó, F. and Fernández, J. (2012). The 2011 Lorca Earthquake slip distribution controlled by groundwater crustal unloading. Nature Geoscience Letters *5*, 821–825.

[López-Comino et al., 2012] López-Comino, J. A., d. L Mancilla, F., Morales, J. and Stich, D. (2012). Rupture directivity of the 2011 Mw 5.2 Lorca Earthquake (Spain). Geophysical Research Letters *31*, L03301.

[Mendoza et al., 2012] Mendoza, L., Kehm, A., Koppert, A., Martín Dávila, J., Gárate, J. and Becker, M. (2012). The Lorca Earthquake observed by GPS: a Test Case for GPS Seismology. Física de la Tierra *24*, in press.

[Vilanova et al., 2012] Vilanova, S. P., Fonseca, J. F. B. D. and Oliveira, C. S. (2012). Ground-Motion Models for Seismic-Hazard Assessment in Western Iberia: Constraints from Instrumental Data and Intensity Observations. Bulletin of the Seismological Society of America *102*, 169–184.

[Vissers and Meijninger, 2011] Vissers, R. L. M. and Meijninger, B. M. L. (2011). The 11 May 2011 earthquake at Lorca (SE Spain) viewed in a structural-tectonic context. Solid Earth *2*, 199–204.

[Zumberge et al., 1997] Zumberge, J. F., Heflin, M. B., Jefferson, D. C., Watkins, M. M. and Webb, F. H. (1997). Precise Point positioning for the efficient and robust analysis of GPS data from large networks. Journal of Geophysical Research *102*, 5005–5017.